Beyond Metal-Arenes: Monocarbonyl Ruthenium(II) Catalysts for Transfer Hydrogenation Reactions in Cancer Cells

Denise Lovison,[a,*] Tobias Berghausen,[a] Sophie R. Thomas,[a] Jonathan Robson,[a] Markus Drees,[b] Christian Jandl,[b] Patrick Mollik,[b] Dominik Halter,[b,c] Walter Baratta[d] and Angela Casini[a,*]

[a] *Chair of Medicinal and Bioinorganic Chemistry, Department of Chemistry, Technical University of Munich, Lichtenbergstraße 4, D-85748 Garching b. München, Germany.*

[b] *Technical University of Munich, School of Natural Sciences, Department of Chemistry, Chair of Inorganic and Metal-Organic Chemistry, Lichtenbergstr. 4, D-85748 Garching Germany.*

[c] *Technical University of Munich, Germany; Catalysis Research Center (CRC), Ernst-Otto-Fischer Str. 1, D-85748 Garching b. München, Germany.*

[d] *Dipartimento di Scienze Agroalimentari, Ambientali e Animali, Università di Udine, Via Cotonificio 108, I-33100 Udine, Italy.*

* Corresponding authors:
E-mail: denise.lovison@tum.de , angela.casini@tum.de

Abstract

With the aim to design new water-soluble organometallic Ru(II) complexes acting as anticancer agents catalysing transfer hydrogenation (TH) reactions with biomolecules, we have synthesized four Ru(II) monocarbonyl complexes (**1-4**) featuring the 1,4-bis(diphenylphosphino)butane (dppb) ligand and different bidentate nitrogen (N^N) ligands, of general formula $[Ru(OAc)CO(dppb)(N^N)]^n$ (n = +1, 0; OAc = acetate). The compounds have been characterised by different methods, including ^1H and ^{31}P NMR spectroscopy, electrochemistry as well as single crystals X-ray diffraction in the case of **1** and **4**. The compounds have also been studied for their hydrolysis in aqueous environment, and for the catalytic regioselective reduction of NAD^+ to 1,4-NADH in aqueous solution with sodium formate as hydride source. Moreover, the stoichiometric and catalytic oxidation of 1,4-NADH have also been investigated by UV-Visible spectrophotometry and NMR spectroscopy. Overall, initial structure-activity relationships could be inferred which point towards the influence of the extension of the aromatic N^N ligand in the cationic complexes **1-3** on the TH in both reduction/oxidation processes. The neutral complex **4**, featuring a picolinamidate N^N ligand, stands out as the most active catalyst for the reduction of NAD^+, while being completely inactive towards NADH oxidation. The compound can also convert pyruvate into lactate in the presence of formate, albeit with scarce efficiency. In any case, for all compounds, Ru(II) hydride intermediates could be observed and even isolated in the case of complexes **1-3**. Together, insight from the kinetic and electrochemical characterization suggests that, in the case of Ru(II) complexes **1-3**, catalytic NADH oxidation sees the H-transfer from 1,4-NADH as the rate limiting step, whereas for NAD^+ hydrogenation with formate as the H-donor, the rate limiting step is the transfer of the ruthenium hydride to the NAD^+ substrate. The latter is further modulated by the presence of di-cationic aquo- or mono-

cationic hydroxo-species of complexes **1-3**. Instead, compound **4**, stable with respect to hydrolysis in aqueous solution, appears to operate via a different mechanism. Finally, the anticancer activity and ability to form reactive oxygen species (ROS) of complexes **1-3** have been studied in cancerous and non-tumorigenic cells *in vitro*. Noteworthy, the conversion of aldehydes to alcohols could be achieved by the three Ru(II) catalysts in living cells, as assessed by fluorescence microscopy. Furthermore, the formation of Ru(II) hydride intermediate upon treatment of cancer cell extracts with complex **3** has been detected by ^{1}H NMR spectroscopy. Overall, this study paves the way to the application of non-arene based organometallic complexes as TH catalysts in biological environment.

Introduction

In biological systems, hydrogenation reactions are usually performed by enzymes using nicotinamide adenine dinucleotide (NAD(P)H) or flavin mononucleotide/dinucleotide as cofactors and hydride sources. In industrial processes, transfer hydrogenation (TH) catalysis is conducted by metal complexes and involves the formation of metal-hydride intermediate enabling hydride transfer from a donor to an acceptor substrate. In this context, when able to perform reactions in aqueous environment, small metal complexes can be viewed not only as potential metalloenzyme mimics, but also as catalysts of biorthogonal reactions in cells, leading to novel applications in catalysis and medicine. For example, catalytic metallodrugs could achieve high efficiency at low dosages and overcome cancer cells resistance through novel modes of actions.

TH reactions in aqueous media were not reported until the mid 1980s[1], and the presence of water seemed to increase catalytic rates, thus, allowing the use of more environmentally friendly solvents. In 1991, Steckhan et al. developed the first series of TH metal catalysts – with $[Cp^*Rh(bipy)Cl]^+$ (bipy = 2,2'-bipyridyl, Figure 1) – being the most active derivative - capable of regenerating regioselectively 1,4-NADH in aqueous media (pH 7, 37 °C) using high concentrations of formate as hydride source[2]. In 2001, Fish et al. obtained structure-activity relationships on $[Cp^*Rh(bipy)Cl]^+$ and derivatives and obtained initial insights into the mechanisms of NADH cofactor regeneration[3]. In 2006, Sadler et al. proposed to exploit the TH properties of Ru(II)-arene complexes of general formula $[(\eta^6$- arene)Ru(X,Y)Cl]PF_6 (X,Y = ethylendiamine, bipy, or acetylacetone, Figure 1) to regenerate NADH[4]. Using this strategy, the concentration of NAD^+ as well as the NAD^+/NADH ratio could be altered, potentially interfering with numerous processes highly controlled in cancer cells, such as energy regulation, DNA repair and transcription, or immunological functions[5, 6]. The catalytic cycle was also studied, showing similar behaviour to complex $[Cp^*Rh(bipy)Cl]^+$. Thus, a number of Ru(II)-arene compounds were further developed[7]. Afterwards, a series of neutral Ru(II) half-sandwich complexes, whereby the choice of the arene and of the chelating ligand has a major effect on the catalytic activity, were shown to regioselectively catalyse the TH of NAD^+ [8-11], and to be able to perform the reaction in cellular environment[12]. Unfortunately, no correlation between activity in NMR experiments and in cells could be observed[13], probably due to catalyst poisoning or side reactions in the cellular environment.

In 2012, Hollman et al. reported a modified heterogenic Rh(III)−Noyori type catalyst capable of reducing NAD^+, proving that the compounds could potentially be used for regeneration of NADH[14]. Further studies on Rh(III)-arene complexes showed that they can reduce NAD^+ to 1,4-NADH and pyruvate to lactate, using formate as the hydride source, under biologically-relevant conditions[11]. Pyruvate is an important intermediate in metabolic pathways in cells; it is the end-product of glycolysis, and is ultimately destined for transport into mitochondria as a pivotal fuel input sustaining the Krebs cycle[15]. Hence, disturbance of pyruvate metabolism is expected to generate metabolic disorder.

More recently, Noyori-type Os(II) compounds of general formula [Os(arene)(TsDPEN)] (TsDPEN, N-(p-toluenesulfonyl)-1,2-diphenylethylenediamine) (Figure 1) were studied for the reduction of pyruvate using formate as a hydride source and under biologically relevant conditions, giving rise to L- lactate or D-lactate with a high enantiomeric excess[13, 16]. The toxicity of the compounds was greatly enhanced upon addition of formate to the cell culture media. Interestingly, Pizarro et al reported on Os(II) complexes bearing picolinate N,O-chelates and studied their reactivity toward catalytic TH of pyruvate, producing quantifiable excess lactate inside cancer cells when using formate as hydride-source[17]. Finally, in 2022, Sungho Yoon et al. described a water-soluble carbene rhodium complex of formula $[(\eta^5$-Cp*)Rh(MDI)Cl]$^+$ [MDI = 1,1′-methylenebis(3,3′-

dimethylimidazolium)] (Figure 1) as catalyst for the reduction of NAD^+ to NADH, highlighting the evidence of the formation of a stable metal hydride intermediate upon its isolation and characterization.[18]

When studying the catalytic activity and cycle of $[(Cp^*)Rh(bipy)Cl]^+$, Fish et al. described the possibility of a reverse reaction, where NADH is oxidized to NAD^+ via formation of a hydride complex[3]. Later in 2012, Ru(II)-arene complexes containing bipyridyl bidentate ligands (Figure 1) were shown to oxidize NADH to generate NAD^+ [19]. Similarly, Cp-based Ir(III) compounds (Figure 1) were also demonstrated to oxidize NADH instead of reducing NAD^+, and were highly active toward A2780 cancer cells, importantly increasing the intracellular NAD^+/NADH ratio[19, 20]. From this study and others[21], it is evident that in general oxidation of NADH itself does not induce cell death but causes an imbalance of the intracellular redox state. Thus, the effect of different biologically relevant components on selected known Ir(III) and Ru(II) catalysts capable of oxidizing NADH was investigated[22]. Density functional theory (DFT) modelling suggests that the mechanism for the oxidation of NADH to NAD^+ involves transfer of hydride from NADH to the Ru(II)/Ir(III) centre via formation of a six-membered transition state, by a coordination site which becomes vacant by a ring-slippage mechanism[23, 24]. Noteworthy, in 2017 Macchioni et al showed that the complex [Cp*Ir(pica)Cl] (pica = picolinamidate, Figure 1) is able to generate active species that efficiently catalyse both NAD^+ hydrogenation and NADH oxidation in aqueous environment[25]. Finally, a series of half-sandwich Os(II) complexes of the type [(arene)Os(iminopyridine)X] (X = Cl or I) (Figure 1) were prepared and their catalytic activity toward oxidation of NADH was successfully tested under physiological conditions[26]. Treatment of cancer cells with some of the derivatives increased the NAD^+/NADH ratio significantly.

Within this framework, we decided to explore a different family of TH organometallic catalysts based on a Ru(II) monocarbonyl scaffold featuring bidentate nitrogen (N^N) and diphosphine (P^P) ligands, of general formula $[Ru(OAc)CO(dppb)(N^N)]^n$ (n = +1, 0; dppb = 1,4-bis(diphenylphosphino)butane). Monocarbonyl ruthenium complexes have attracted a great deal of attention in homogeneous catalysis due to their ability to promote several transformations, including in the transfer hydrogenation and hydrogenation of a number of carbonyl compounds[27-32]. However, to the best of our knowledge, they have never been tested in TH reactions with the NAD^+/NADH couple. Recent studies also showed that this family of compounds are endowed with antiproliferative activity in cancer cells[33-37]. Therefore, we synthesized three Ru(II) monocarbonyl compounds (Scheme 1, complexes **1-3**) featuring the same bidentate phosphine 1,4-bis(diphenylphosphino)butane (dppb) but different N^N ligands - namely ,2'-bipyridine (bipy), 1,10-phenanthroline (phen) and pyrazino[2,3-*f*][1,10]phenanthroline (pzphen) - to explore the effects of the different aromatic scaffolds on the catalytic activity of the compounds. Moreover, inspired by the aforementioned previous work on Ir(III)-arene complexes featuring the picolinamidate (pica) ligand[25], we synthesized the corresponding monocarbonyl analogue (Scheme 1, complex **4**). The compounds have been characterized by different methods, including single crystal X-ray diffraction (SC-XRD) analysis, and their reactivity towards the NADH/NAD^+ pair studied by UV-visible absorption, fluorescence, as well as ^1H and ^{31}P NMR spectroscopies. The Ru(II) complexes demonstrated to be active as catalysts for the regioselective regeneration of 1,4-NADH by reduction of NAD^+ with formate as hydride source in aqueous media, with compound **4** as the most active. The latter was also able to convert pyruvate to lactate, although with moderate catalytic activity. Moreover, the Ru(II) complexes **1-3** were able to oxidize NADH to produce NAD^+ both in stoichiometric and catalytic conditions. The isolation of the hydride complexes was attainable in the case of catalysts **1-3**, and initial mechanistic insights based on kinetic, electrochemical and DFT studies shed light into the catalytic activities of the titled complexes. Compounds **1-**

3 showed marked antiproliferative activities in a small panel of human cancer cells in comparison to non-tumorigenic ones *in vitro*. Moreover, formation of reactive oxygen species (ROS) could also be detected in cells. Notably, the conversion of aldehydes to alcohols by the Ru(II) catalysts **1-3** was studied in living cells by fluorescence microscopy using a BODIPY fluorogenic substrate. Finally, evidence of Ru(II) hydride complex formation was achieved in cell extracts treated with compound 3 by ^{1}H NMR spectroscopy.

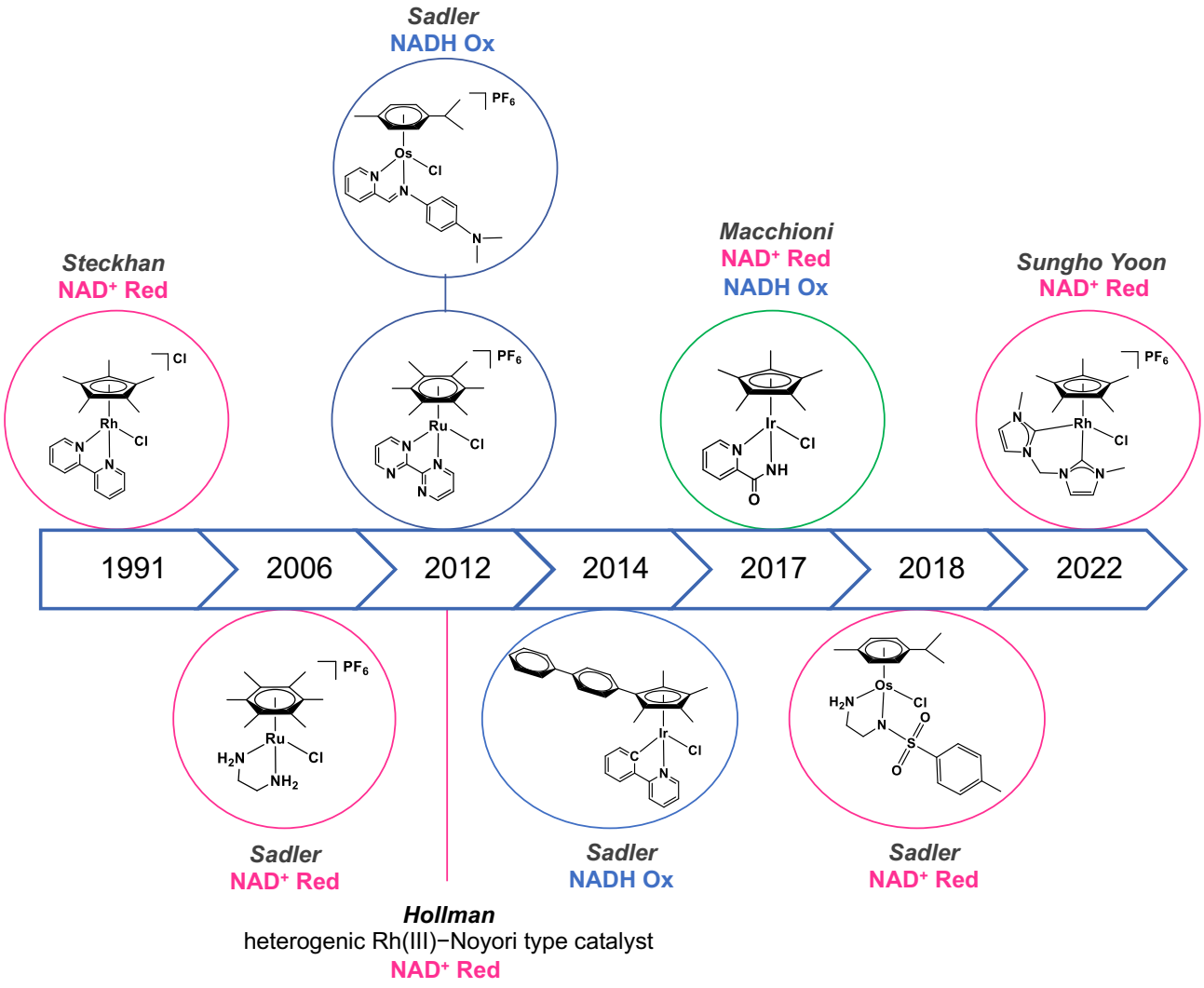

Figure 1 – Timeline of milestones in the development of transfer hydrogenation metal-arene catalysts for NAD$^+$ reduction/NADH oxidation in aqueous media.

Results and discussion

Synthesis and characterization of Ru(II) complexes

Complexes **1**-**4** were synthesized as previously reported in literature for compound **2** (Scheme 1)[37]. Briefly, for the cationic complexes **1**-**3**, the acetate diphosphine complex [Ru(η^1-OAc)(η^2-OAc)(CO)(dppb)] (dppb = 1,4-bis(diphenylphosphino)butane) was treated with 1 equiv. of the chosen N^N ligand, namely 2,2'-bipyridine (bipy), 1,10-phenanthroline (phen) and pyrazino[2,3-*f*][1,10]phenanthroline (pzphen), in MeOH at 60 °C. For complex **4** the same reaction was conducted at 80 °C in EtOH using picolinamidate (pica) as ligand, in order to afford a neutral complex by displacement of one acetate ligand. In addition, the corresponding non

carbonylic compound **2A** was obtained from the diacetate analogue [Ru(η^2-OAc)$_2$(dppb)][32], after reacting with 1,10-phenanthroline in methanol at 60 °C. All the complexes display high solubility and stability in several media, including alcohols (MeOH and EtOH), chloroform, dichloromethane, acetone, dimethylformamide and dimethylsulfoxide. Furthermore complexes **1**-**3** and **2A** exhibit good water solubility, while complex **4** (1 mM) was solubilised in water after being first dissolved in a 20% (v/v) of dimethylformamide.

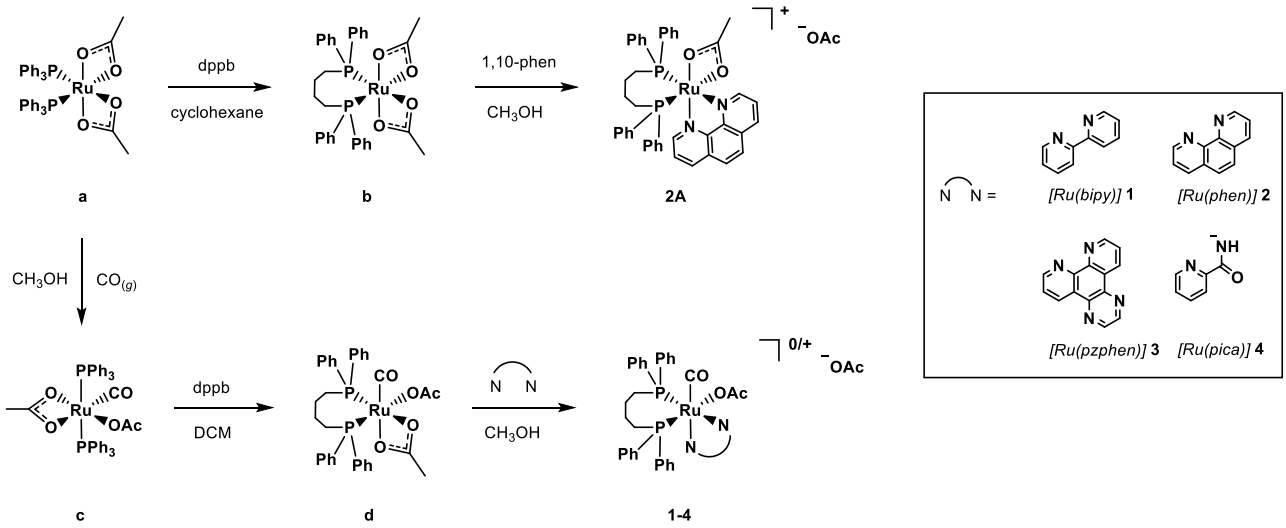

Scheme 1. Synthetic routes followed to obtain the monocarbonyl Ru(II) complexes **1**-**4** and **2A**.

X-ray diffraction analysis

The full characterization of the complexes was accomplished by ^{1}H, ^{13}C and ^{31}P NMR spectroscopy (ESI Figures S1-S12), as well as by single crystal X-ray diffraction (SC-XRD) for **1** and **4** (Figure 2, Table 1), while the crystal structure of **2** has been previously reported[37]. Crystals suitable for analysis were obtained by slow diffusion of diethyl ether into a solution of the Ru complex in dichloromethane (ESI Tables S1-S2). It is evident from the bond angles between the ligands and Ru(II) center (Table 1) that both complexes show a marginally distorted octahedral geometry, as previously observed for complex **2**[37]. The strong *trans* influence of the diphosphine and CO ligands is noticeable in both molecular structures with increased lengths of the Ru1-N1 bonds, as well as the Ru1-O2 bond (Table 1). The latter suggests the facile dissociation of the acetate ligand, as previously reported for complex **2**[37].

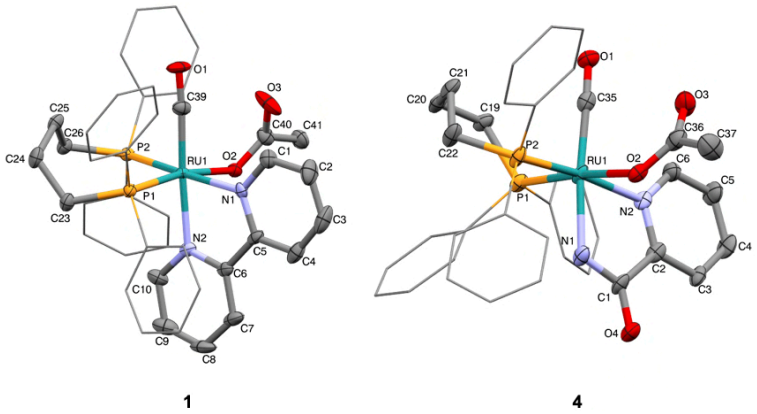

1 **4**

Figure 2 – Molecular structures of **1** and **4** as determined by SC-XRD. Ellipsoids are displayed at the 50% probability level. Hydrogen atoms and the counter anion of **1** have been omitted for clarity, as well as the simplification of the phenyl groups as wireframes.

Table 1 – Selected distances and bond angles for complexes **1** and **4** obtained from SC-XRD experiments.

Complex 1				**Complex 4**			
Bond lengths (Å)		Bond angles (°)		Bond lengths (Å)		Bond angles (°)	
Ru1-C39	1.847(4)	C39-Ru1-N1	97.64(14)	Ru1-C35	1.885(8)	C35-Ru1-N2	95.7(3)
Ru1-N1	2.101(3)	C39-Ru1-O2	95.87(13)	Ru1-N2	2.134(6)	C35-Ru1-O2	95.9(3)
Ru1-N2	2.151(3)	P1-Ru1-P2	100.58(3)	Ru1-N1	2.088(6)	P1-Ru1-P2	94.86(7)
Ru1-P1	2.3435(9)	N1-Ru1-N2	77.64(11)	Ru1-P1	2.312(2)	N1-Ru1-N2	77.0(2)
Ru1-P2	2.3717(10)	C39-Ru1-N2	175.27(14)	Ru1-P2	2.3087(19)	C35-Ru1-N1	172.7(3)
Ru1-O1	1.160(4)			Ru1-O1	1.141(9)		
Ru1-O2	2.117(2)			Ru1-O2	2.156(5)		

Hydrolysis studies of ruthenium complexes and pK_a determination

The chemical reactivity of metal complexes in biological conditions generally occurs via the hydrolysis of labile monodentate ligands. In previous works, we demonstrated by NMR spectroscopy that for this class of Ru(II) complexes a water molecule displaces the acetate ligand, resulting in the formation of the aquo- or hydroxo-species depending on the examined pH, in accordance with DFT calculations showing stabilizing H-bonds between the acetate oxygen atoms and the hydrogen atoms of incoming water molecules[36, 37]. To elucidate the aqueous behaviour and the rate of the hydrolysis process for the new complexes, ^{1}H NMR kinetic studies were carried out in deuterated PBS media at both pD 7.4 and 6.3 within 12 hours (Figure 3A). The slightly acidic pH was selected since it is relevant to cancer cells.

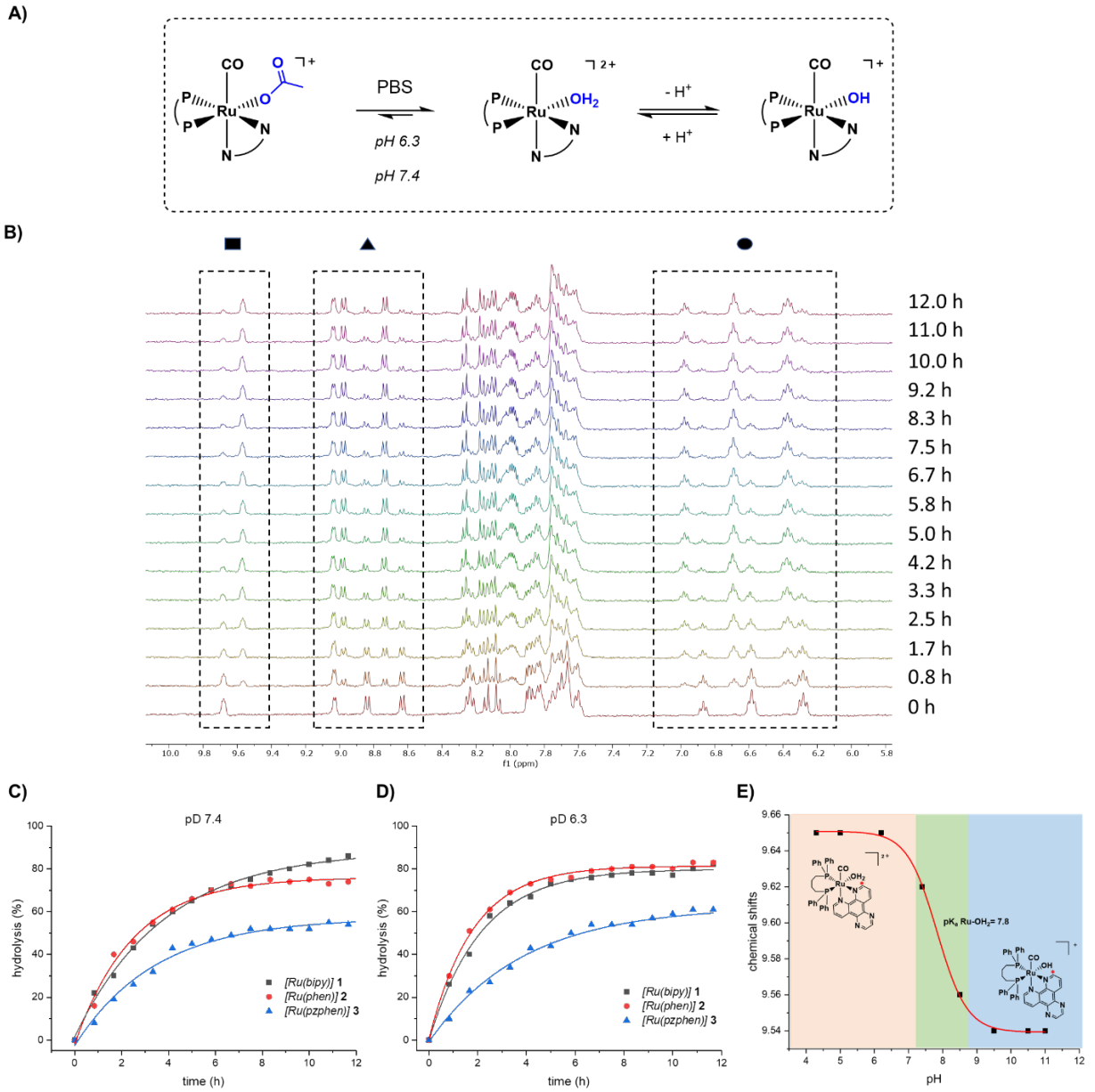

Figure 3. A) Hydrolysis of the Ru(II) monocarbonyl complexes studied in this work. B) Stacked ^{1}H NMR spectra of a solution of complex **2** in PBS pH 6.3. The formed aquo-specie increases over 12 hours and originates new pattern of signals for the ortho (square) and other aromatic (triangle) protons of the phenanthroline ligand, and for the dppb phenyls protons (circle). Hydrolysis kinetics plotted over time at different pDs: C) 7.4 and D) 6.3. E) Plot of the chemical shift changes of the resonances from δ 9.65 to 9.54 ppm corresponding to the most deshielded *otho* proton of the pzphen ligand for complex **3** (red asterisk). The pH was increased in the range of ca. 4-11.

The ^{1}H NMR spectra of the compounds exhibited new pattern of signals (Figure 3B and Figures S13-S15) which demonstrated the formation of a second aquo-specie over 12 h mainly distinguishable in the aromatic region, whereby the chemical shifts of the nitrogen donor aromatic ligand and the phenyls of the diphosphine were subjected to up-field and down-field shifts, respectively. The replacement of the coordinated OAc with a water molecule is also proven by the decrease over time of the acetate singlet at 1.63 ppm (ESI Figure S13-S15). Compounds **1-3** undergo partial hydrolysis reaching an equilibrium between the acetate and

the aquo forms after 12 hours. Depending on the pH, the compounds show different trends: after 12 hours at pH 7.4, complex **1** reaches a plateau, being converted to the aquo-form to the extent of 86%, the highest percentage of conversion compared to the other complexes (Figure 3C). At the same pH, both complexes **2** and **3** reached a plateau after 7.5 hours with 72% and 52% of conversion, respectively. Interestingly, at pH 6.3 all the complexes showed approximately the same percentage of hydrolysis as at pH 7.4 after 12 hours, although exhibiting a slightly faster trend toward the equilibrium (Figure 3D and Figures S13-S15). Overall, complexes **1** (bipy) and **2** (phen) undergo more pronounced hydrolysis with respect to **3** (pzphen). Conversely, complexes **4** and **2A** did not show any hydrolysis process at both pHs and are stable over a period of 24 hours (data not shown).

Following the Ru-OAc cleavage, the changes in the ^{1}H NMR chemical shifts of the coordinated N^N ligand of complexes **1**-**3**, were followed upon increase in pH over the range 4-11 in deuterated PBS solutions, as previously reported in literature[17, 38-43]. The monitored aquo/hydroxo signals belonging to the N^N ligand protons shifted to higher field with increase in pH, while the signals attributable to the non-hydrolysed acetate complexes remained unchanged with varying pH. The chemical shifts of aquo/hydroxo species were plotted against pH and the data were fitted to the Henderson-Hasselbach equation, from which the pK_a values of the coordinated water were determined. The collected data yielded pK_a values of 8.7, 8.4 and 7.8 for complexes **1**,**2** and **3**, respectively (Figure 3E and ESI Figures S16). These data suggest that the extension of the N^N chelating ligand, as in the case of complex **3**, reduces the electron density on the metal, lowering the pK_a of the coordinated water up to 0.9 pK_a units (Figure 3E). Furthermore, the pK_a values indicate that at physiological pH complexes **1**-**3** would be present in their more reactive aquo-form, although to a lesser extent for the pzphen derivative **3**.

Catalytic NAD^+ reduction

The regiospecific reduction of NAD^+ to 1,4-NADH was investigated by ^{1}H NMR spectroscopy using complexes **1**-**4** and **2A** as catalysts and potassium formate as hydride source in deuterated PBS at both pD 6.3 or 7.4, at room temperature (Figure 4). The molar ratios of [Ru] catalyst : NAD^+ : HCOOK varied while the concentration of [Ru] was kept constant (see Experimental for details). Only for the non-water soluble complex **4**, the samples were prepared with a 20% (v/v) of deuterated DMF. The stability of NAD^+ and NADH in DMF was previously assessed, as well as the possibility of DMF affecting the rate of the catalysis. As comparison, the reaction catalysed by complex **1** was also tested in the same 20% DMF solution, demonstrating no interferences with the rate of the catalytic system compared to the one in 100% aqueous PBS. The transfer hydrogenation reactions were followed by ^{1}H NMR kinetic experiments over a time interval of 48 hours (Figure 4B) and the relative proportions of the oxidized and reduced forms of the coenzyme were determined by integration of the H2 and J2 signals (see full assignment in ESI Figure S17). The catalytic cycle can start directly from the Ru(II) complex or from its aquo-species which can react with formate to afford the hydride ruthenium complex via *β*-hydride elimination accompanied by CO_2 evolution. The hydride complex is then able to hydrogenate NAD^+ liberating 1,4-NADH and regenerating the Ru(II) aquo-specie (Figure 4A).

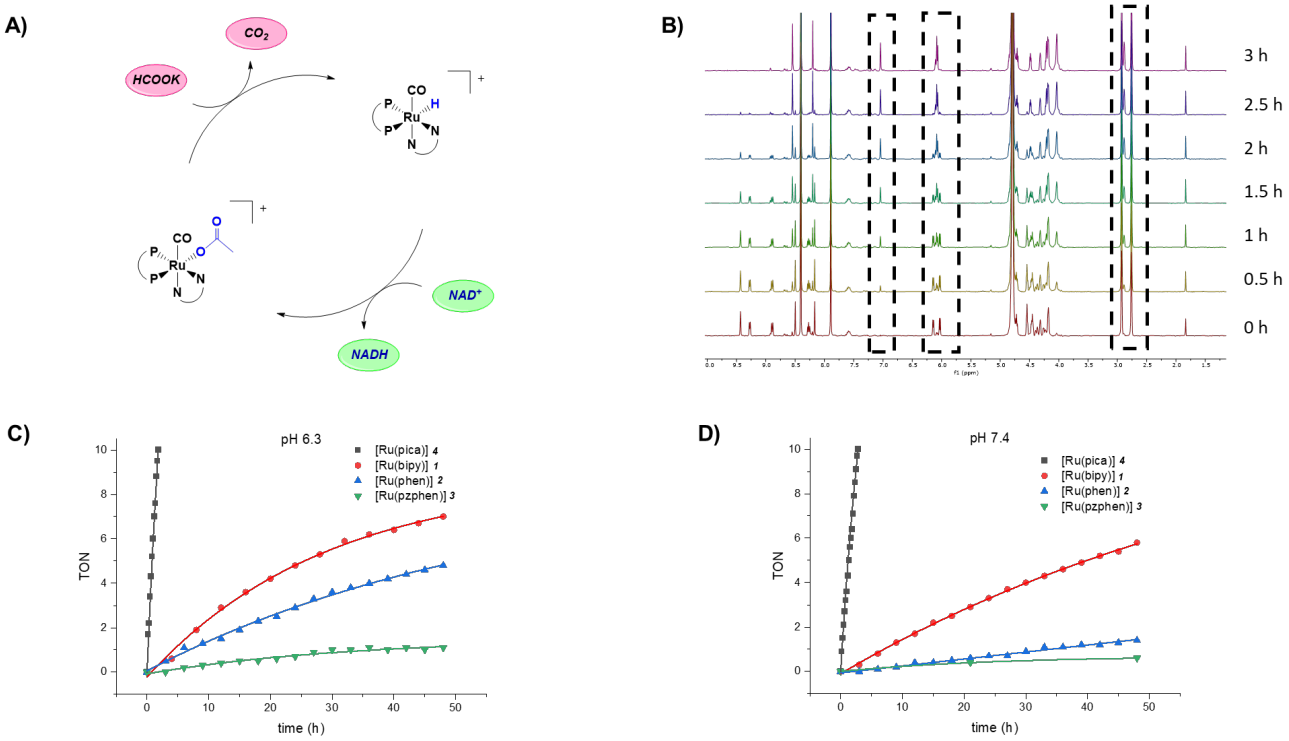

Figure 4. A) Proposed catalytic pathway for the reduction of NAD^+ accomplished by complexes **1**-**4** and **2A** in PBS at pH 7.4 and 6.3. B) Stacked ^1H NMR kinetics of the reduction of NAD^+ performed by complex **4** showing the regioselective formation of 1,4-NADH (in deuterated PBS buffer at pH 7.4 over 3 h with molar ratios of catalyst : NAD^+ : HCOOK = 1:10:50). Trends of conversion *vs* time at pH C) 6.3 and D) 7.4.

The catalytic activity of complexes **1**-**4** towards NAD^+ reduction showed a marked dependence on both the N^N aromatic ligand and the pH (Figures 4C and 4D). TOF and TON numbers at different pH values are summarized in Table 2. In detail, cationic complexes **1-3** are poor active catalysts with the rate of NAD^+ hydrogenation increasing by reducing the extension of the N^N ligand in the order bipy > phen > pzphen. On the other hand, the neutral complex **4** featuring the pica ligand is the most efficient catalyst of the series, while being stable towards acetate hydrolysis. In fact, at molar ratios [Ru] : NAD^+ : HCOOK = 1:10:50, at pH 6.3, complex **4** exhibited the highest rate of conversion, completing the catalysis in only 1.8 hours (TOF = 6.08 h^{-1}). Overall, the substitution of the pzphen ligand (**3**) with picolinamidate (**4**), resulted in a 46-fold increase in catalytic activity. In general, these data points towards a different mode of TH for compound **4** with respect to the N^N family of Ru(II) complexes. It should also be noted that the affinity of the NAD^+ substrate for the cationic hydrides of complexes **1-3** (Scheme 2) should be reduced due to unfavourable electrostatic interactions in comparison to the neutral hydride of compound **4**. The pH also plays an important role in affecting the rate of conversion and overall catalytic efficiency of all compounds, whereby the catalytic rate of conversion at pH 7.4 is ca. 2-fold lower with respect to pH 6.3 (Table 1). Complex **2A**, did not show any catalytic activity toward the hydrogenation of NAD^+ independently on the pH (data not shown).

Table 2. Catalytic activity for the reduction of NAD^+ catalysed by complexes **1**-**4** and **2A** over 48 h at pH 6.3 and 7.4, where [Ru] : [NAD^+] : [HCOOK] = 1 : 10 : 50.

Complexes	***TOF (h^{-1})***	***TON***

	pH 6.3	pH 7.4	pH 6.3	pH 7.4
[Ru(bipy)] (***1***)	0.20	0.13	7.0	5.8
[Ru(phen)] (***2***)	0.12	0.03	4.8	1.4
[Ru(pzphen)] (***3***)	0.03	0.01	1.1	0.6
[Ru(pica)] (***4***)	6.08[(a)]	3.76[(b)]	10[(a)]	10[(b)]

[(a)] catalytic cycle completed in 110 min; [(b)] catalytic cycle completed in 170 min.

Full characterization of the hydride derivatives **1H-3H** was obtained by reacting complexes **1-3** with 3 equiv. HCOOK in PBS pH 7.4 and isolating the hydrides upon addition of $NaPF_6$ (Scheme 2), while the formation of **4H** was observed only in solution and the compound could not be isolated due to instability in the solid state. Hydride formation could not be assessed in the case of complex **2A**, likely due to the fact that it cannot easily liberate acetate by hydrolysis.

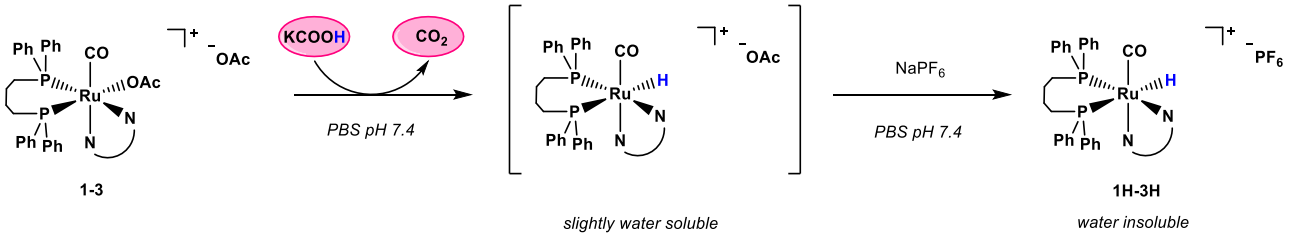

Scheme 2. Synthesis of the Ru(II) hydride complexes **1H**-**3H**.

Notably, the isolation of the ruthenium hydride species was only possible in aqueous media: the same procedure carried out in other organic solvents (methanol, acetone, dimethylsulfoxide, dichloromethane and DMF) did not lead to the formation of the intended hydride derivatives. Interestingly, in DCM the addition of HCOOK to complexes **1-3** leads to the exchange of the acetate bound ligand with formate (ESI Figures S19-S20). It is therefore hypothesized that water addition is a crucial step to trigger β-hydride elimination. The full characterization of the isolated hydride derivatives **1H-3H** was accomplished by ^{31}P, ^{1}H and ^{13}C NMR spectroscopy. It is worth noting the marked shift of the dppb phosphorus signals in the ^{31}P NMR upon formation of the hydride derivative, with respect to the acetate precursors. While for instance complex **2** exhibits two doublets at δ 32.2 and 29.3 ppm in CD_3OD, the corresponding hydride derivative **2H** (Fig. 5A) displays two shifted signals at δ 56.1 and 11.2 ppm for the P atoms *trans* to N and H, respectively (Figure 5B). The presence of the hydride *trans* to a P atom was also confirmed by ^{1}H NMR, whereby a doublet of doublet at δ -6.05 ppm could be detected (Figure 5C). The same behaviour was observed for complexes **1H** and **3H** (ESI, Figures S21-S26).

To prove that the provenance of the hydride came right from formate upon β-hydride elimination and not from the solvent, we also isolated the deuteride analogue of complex **2H**, after reacting complex **2** with deuterated sodium formate in non-deuterated water, obtaining the straightforward ^{31}P chemical shifts characteristic of the formation of the ruthenium deuteride/hydride derivative. However, the ^{1}H NMR spectrum

shows a 10% of the hydride species, probably due to the scrambling with the solvent to a lesser extent (Figures S27-S28). The SC-XRD structure of the Ru(II) hydride complex **2H** has also been obtained (Figure 5D, and ESI Table S3). The molecular structure of **2H** shows a slightly disordered octahedral geometry, similar to complex **2**[37], except with a marginally larger P1-Ru1-P2 bite angle (**2H**: 101.52 (3)°; **2**: 94.08(3)°, most likely due to the smaller size of the hydride compared to the OAc ligand. The Ru1-P1 bond, *trans* to the hydride, increases in length for **2H** compared to the same bond in **2** (2.4462(8) Å *vs.* 2.3322 (12) Å, respectively), which can be attributed to the strong *trans* influence of the hydride[44]. The Ru1-H4 bond length is comparable to that found for a $[Ru(H)(bpy)_2(PPh_3)](PF_6)$ complex previously characterised by SC-XRD[45].

A)

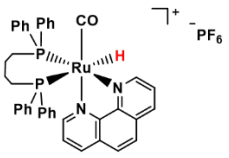

[Ru(phen)H] (**2H**)

B)

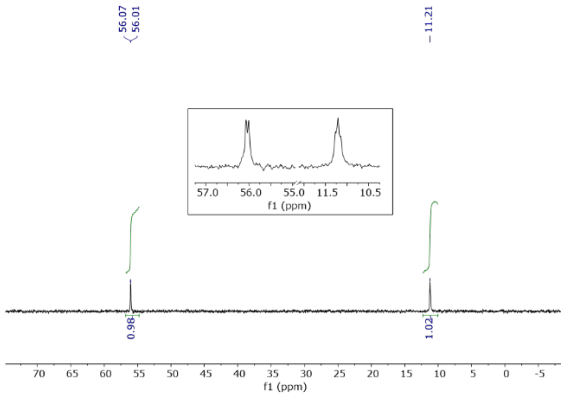

C)

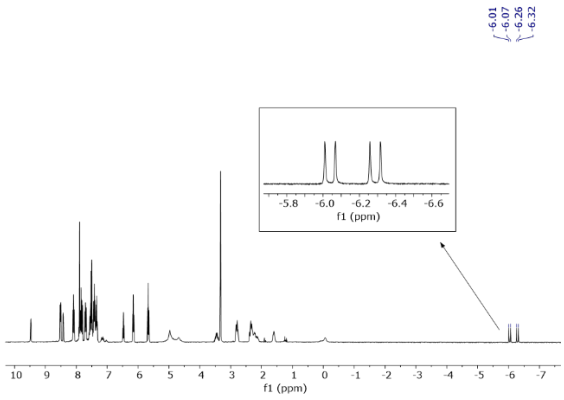

D)

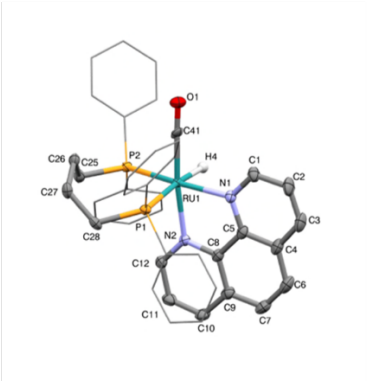

Figure 5. A) Chemical structure of the Ru(II) hydride complex **2H**; B) ^{31}P-NMR spectrum of complex **2H** in CD_3OD; C) ^{1}H-NMR spectrum of complex **2H** in CD_3OD. Inset shows the hydride signals. D) Molecular structure of **2H** as determined by SC-XRD, ellipsoids are displayed at 50% probability. The remaining hydrogen atoms and counterion have been omitted, and the phenyl groups are simplified as wireframes for clarity.

A second series of experiments was performed in order to investigate the dependence of the reaction rate for the catalytic reduction of NAD^+ on the formate concentration and as a function of pH. The plot of the data obtained for complex **4** shows a strong dependence of the turnover number (TON) and turnover frequency (TOF) on the formate concentration (Figure 6 and Table 3). Thus, TOF numbers were found to markedly increase upon increase in the concentration of HCOOK from 25 to 200 equiv. (Figure 6C). Moreover, an enhancement in catalytic activity was also observed at the most acidic pH value for all the tested HCOOK concentrations, reaching TOF numbers as high as 17.3 h^{-1} and completing the catalysis in 40 min. In contrast, complexes **1**-**3** were not affected by differences in formate concentration, exhibiting the same trend reported for 50 equiv. of the reducing source (see Figure S29). These results indicate that the NAD^+ reduction catalysed by complex **4** is first-order with respect to HCOOK, which parallels the observations of Macchioni et al. for the Ir(III)-arene complex featuring the same pica ligand[25]. Moreover, it is reasonable to assume that the catalytic mechanism involving complex **4** might be different with respect to the one of the other monocarbonyl Ru(II) complexes.

Table 3. Kinetic data for the reduction of NAD^+ catalysed by complex **4** (10%) at pH 7.4 and 6.3 at room temperature, where [Ru] : [NAD^+] : [HCOOK] = 1 : 10 : X.

	TOF (h^{-1})	
HCOOK equiv.	**pH 6.3**	**pH 7.4**
25	2.74	2.31
50	6.08	3.76
100	9.03	5.82
200	17.3	10.4

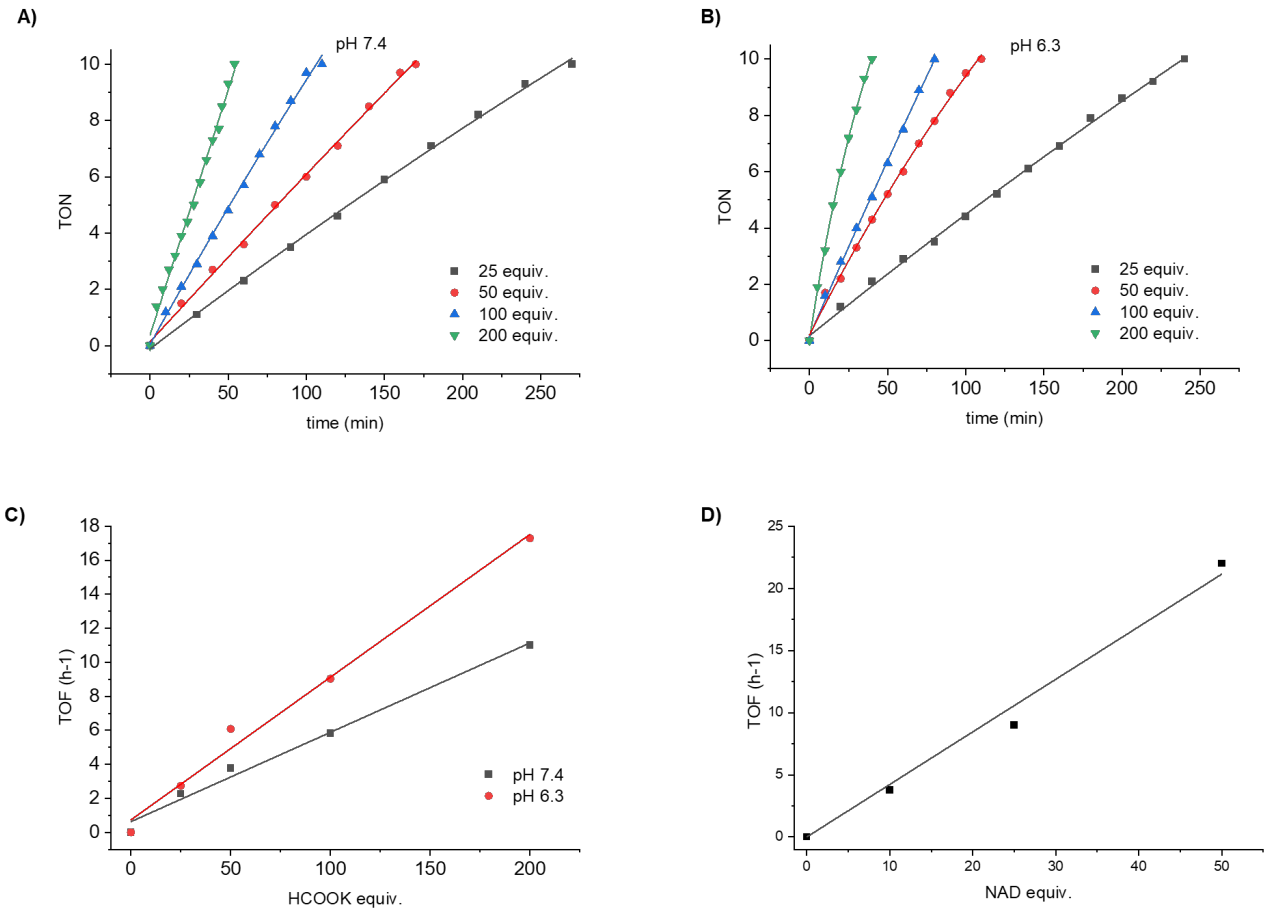

Figure 6. Trends of turnover number (TON) *vs* time at A) pH 7.4 and B) pH 6.3 for complex **4** at different HCOOK concentrations (25, 50, 100, 200 equiv.). C) Plot of the turnover frequency (TOF) for complex **4** (10%) against the HCOOK equiv. used for the catalytic reduction of NAD^+ at both pHs. D) Plot of the turnover frequency (TOF) for complex **4** against NAD^+ equiv. keeping the NAD^+ : HCOOK ratio constant (1 : 4) at pH 7.4.

In further studies concerning complex **4**, TOF was also found to increase by increasing the concentration of NAD^+ with respect to the catalyst, while the ratio between NAD^+ and the reducing agent was kept constant ([Ru] : NAD^+ : HCOOK = 1 : X : 4X, where X = 10, 25, 50) (Figure 6D), reaching a TOF value of 22.8 h^{-1} for 50 equiv. of NAD^+. This means that the rate of conversion is strictly related to the concentration of the substrate. This is further demonstrated by the comparison between the two kinetics [Ru] : [NAD^+] : HCOOK = 1 : 50 : 200 and [Ru] : [NAD^+] : HCOOK = 1 : 10 : 200, whereby the first one exhibits a TOF number 2-fold higher than the same reaction carried out with10 equiv. NAD (Figure 6D).

Mechanistic evaluation

In order to shed light into the mechanism of the hydride transfer in the conversion of NAD^+ to NADH, we splitted the reactions into two steps: i) the formation of the Ru-H complexes, and ii) the transfer of the hydride to NAD^+. Complex **1** was selected as representative example and reacted with a stochiometric amount of HCOOK, leading to the quantitative formation of complex **1H** in solution as shown by ^1H NMR spectroscopy (Figure S30). In this first step, no relevant differences where observed for the formation of the Ru-H derivatives concerning complexes **1**-**3**. Following addition of one equivalent of NAD^+, complex **1H** was not able to transfer

the hydride to the coenzyme over 24 hours (ESI Figure S31), and only after addition of excess formate (20 equiv.) the complete conversion of NAD^+ to NADH was achieved within 8 hours (ESI Figure S32). The same experiment was performed adding an excess of NaOAc (non-hydride donor) instead of HCOOK to solutions of **1H.** Surprisingly, the hydride was transferred to NAD^+ forming NADH, although to a lesser extent (50% conversion) within 24 h, compared to the same reaction with HCOOK (Figure S33). Based on these results, it is therefore reasonable to hypothesize that the transfer of the hydride to the substrate is the rate limiting step of the catalysis for compounds **1**. Instead**,** when NAD^+ (1 equiv.) was added to a solution of complex **4H** with no excess of formate, the formation of NADH was achieved in less than 1 hour (Figures S34) confirming the high catalytic efficiency of this compound and that it is likely to act via a different mechanisms compared to **1-3**.

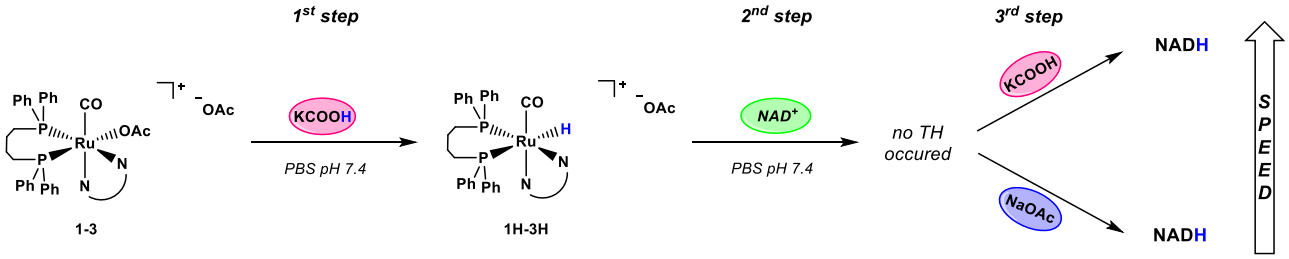

Scheme 3. Reaction scheme describing the hydride formation from **1-3** and the transfer of hydride from Ru-H complexes **1H-3H** to NAD^+ before and after addition of excess formate or acetate as hydride source.

DFT calculations were carried out starting from the acetate complexes **1** and **2**, respectively, to follow the formate addition and CO_2 release to form the hydride complex, following by the transfer of the hydride to NAD^+ as presented in Scheme 3 with some additional transition and ground states. Scheme 4 shows the envisaged reaction steps, including the abbreviations of the ground and transition states, and Table 4 the respective energies. Figure S35 shows the energy profile of our mechanism for the two complexes. The exchange from acetate to formate is endergonic at 298 K with a ΔG value of 3.2 kcal/mol for **1** to **1F** and 2.7 kcal/mol for **2** to **2F**. Afterwards, we calculated the relevant transition states for the transfer of the hydride from the formate to the Ru(II) center as suggested by the deuterated sodium formate studies above. The barrier heights are rather high (29.1 kcal/mol for **1F** to **1H** / 29.3 kcal/mol for **2F** to **2H**, Figure S35). We, therefore, included also the intermediates of the formate complexes where the formate is coordinated via the H atom and not via the O atom, similarly to what predicted in the transition state. As expected, the isomers **1F*** and **2F*** are higher in energy with +27.5 kcal/mol and 28.5 kcal/mol above **1F** and **2F**, respectively (Figure S35). However, these "hypotetic" isomers can be regarded as pre-complexes before reaching the H-transfer TS from the formate ligand via CO_2 formation to the Ru-H species. Thus, **TS1F** is 1.6 kcal/mol higher than **1F***, and TS2F is only 0.9 kcal/mol higher than **2F***. The formation of the hydride species **1H** and **2H** is still higher in energy than the formate complexes **1F** and **2F**. **1H** is 19.1 kcal/mol higher than **1F** and **2H** is 19.7 kcal/mol higher than **2F**. To get the energy down, the H transfer from the Ru complex to NAD^+ has to occur to form the most stable isomer 1,4-NADH, accompanied by the addition of another formate salt in order to regenerate the catalytic system. With that, the energy of the final step goes down by -17.3 kcal/mol from the hydride species **1H** to **1F**, and by

-18.0 kcal/mol from **2H** to **2F** with the hydration of NAD^+. It can be concluded that the scarce reactivity of **1** and **2** can be seen in the rather non-favorable energies along our TH pathway.

Table 4. Calculated ΔG values of species shown in Scheme 4. The acetate ion serving as counter ion is omitted in the calculation.

Ru(II) complex	***Stages during the mechanism of TH***			
	Acetate complex	**Formate complex**	**Hydride complex**	**Formation of formate complex after TH to NAD^+**
1 [Ru(bipy)]	0.0 **(1)**	+3.2 **(1F)**	+22.3 (**1H**)	+4.9 (**1F**+1,4-NADH)
2 [Ru(phen)]	0.0 **(2)**	+2.7 **(2F)**	+22.4 (**2H**)	+4.4 (**2F**+1,4-NADH)

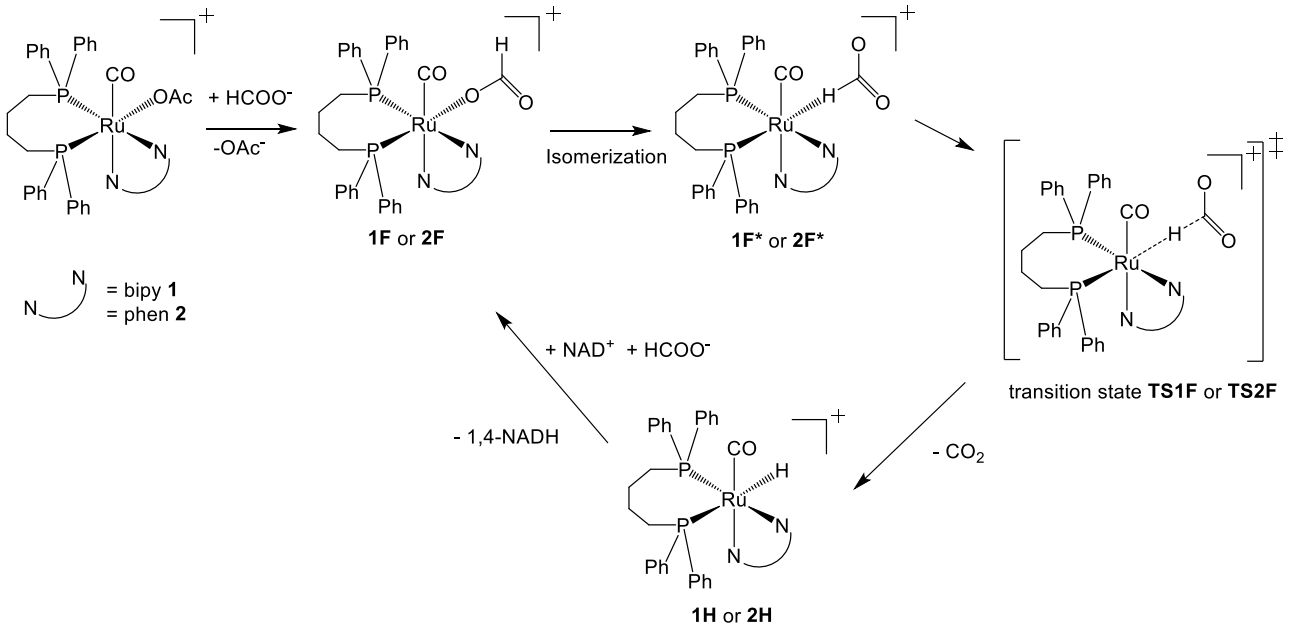

Scheme 4 - The possible mechanism of TH starting from complexes **1** and **2** divided into three steps. (a) acetate to formate substitution; (b) hydride formation in parallel to CO_2 release c) transfer hydrogenation to NAD^+. All energies reported are on the ΔG scale.

Catalytic reduction of pyruvate

The catalytic reduction of pyruvate to lactate using our Ru(II) complexes was studied by ^{1}H NMR spectroscopy in deuterated PBS (pH 7.4). While complexes **1**-**3** showed no conversion of pyruvate, [Ru(pica)] (**4**) showed low catalytic activity, and after 48 h less than 25% conversion was achieved (Figure S36).

Stoichiometric oxidation of NADH

Afterwards, the catalytic activity of the Ru(II) monocarbonyl complexes was challenged towards NADH oxidation. In this case, following Ru(II) hydride formation, NADH is converted into its oxidized form NAD^+ (Figure 7A). Indeed, when NADH is added to a PBS solution (pH 7.4) of complexes **1**-**3** (0.2 M) the formation of the Ru(II) hydride derivatives **1H**-**3H** is observed by ^1H and ^{31}P NMR spectroscopy (Figure 7B-C). Interestingly, no reactivity could be observed in the case of the neutral complex **4** and of complex **2A**. Figures 7A and 7B report the representative ^1H NMR and ^{31}P NMR spectra of a sample of complex **3** with NADH (2 equiv.) in deuterated PBS buffer (pH 7.4) recorded after 3 h. The results show the formation of new proton signals (δ = 9.46, 9.26, 8.94 and 8.24 ppm) attributable to the hydrogen atoms of the NAD^+ nicotinamide ring (see ESI Figure S17 for the assignment), as well as a doublet of doublet around -4.7 ppm for the Ru-H species. The formation of **3H** was further confirmed by the ^{31}P NMR experiment showing the typical chemical shifts attributable to the formation of the ruthenium hydride derivative in the range 10-60 ppm (Figure 7B).

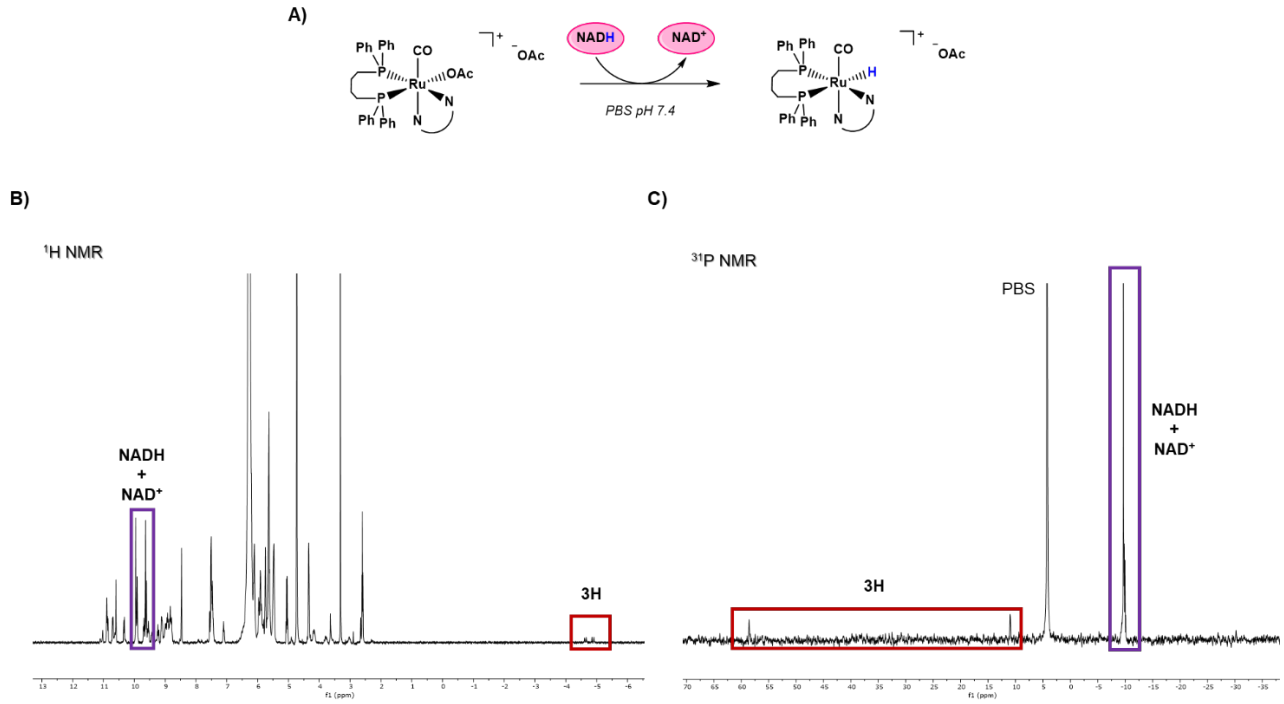

Figure 7. A) Reaction scheme for the interaction between the Ru(II) monocarbonyl complexes and 1,4-NADH (2 equiv.) in deuterated PBS pH 7.4. B) ^1H NMR and C) ^{31}P NMR spectra of [Ru(pzphen)] (**3**) reacting with 1,4-NADH in PBS pH 7.4.

The dehydrogenation of NADH promoted by the Ru(II) monocarbonyl complexes was also investigated by UV-Visible spectrophotometry following the NADH absorption band at 340 nm. Upon stoichiometric addition of the ruthenium compounds, the band decreases over 48 hours at room temperature. The kinetics experiments were carried out in PBS buffer at physiological pH (7.4), as well as at slightly acidic and basic pH (6.3 and 9, respectively) (see Figure 8 and Figures S37-S40). Interestingly, the obtained data suggest that the Ru(II) complexes **1**-**3** and **2A** are all able to oxidize NADH to different extents. In general, the NADH oxidation reaction proved to be faster at the more acidic pH 6.3, reaching the total conversion to NAD^+ in ca. 48 hours.

At pH 7.4 the conversion demonstrated to be much slower and never reached completion, and the reaction was practically negligible at the highest pH 9 (Figure 8 C-E). These marked differences in reactivity might be due to the interconversion of the aquo and hydroxo species in the pH range 6.3-9.0. The different N^N ligands also affect the rate of conversion of NADH to NAD^+, with complex **3** (pzphen) being more reactive than **1** (bipy) and **2** (phen) (Figure 8C-E). The activity of the non-carbonylated complex **2A** showed a similar trend vs pH compared to the other complexes, although most likely it works via a different mechanism due to the presence of the chelating acetate ligand (Figure S40).

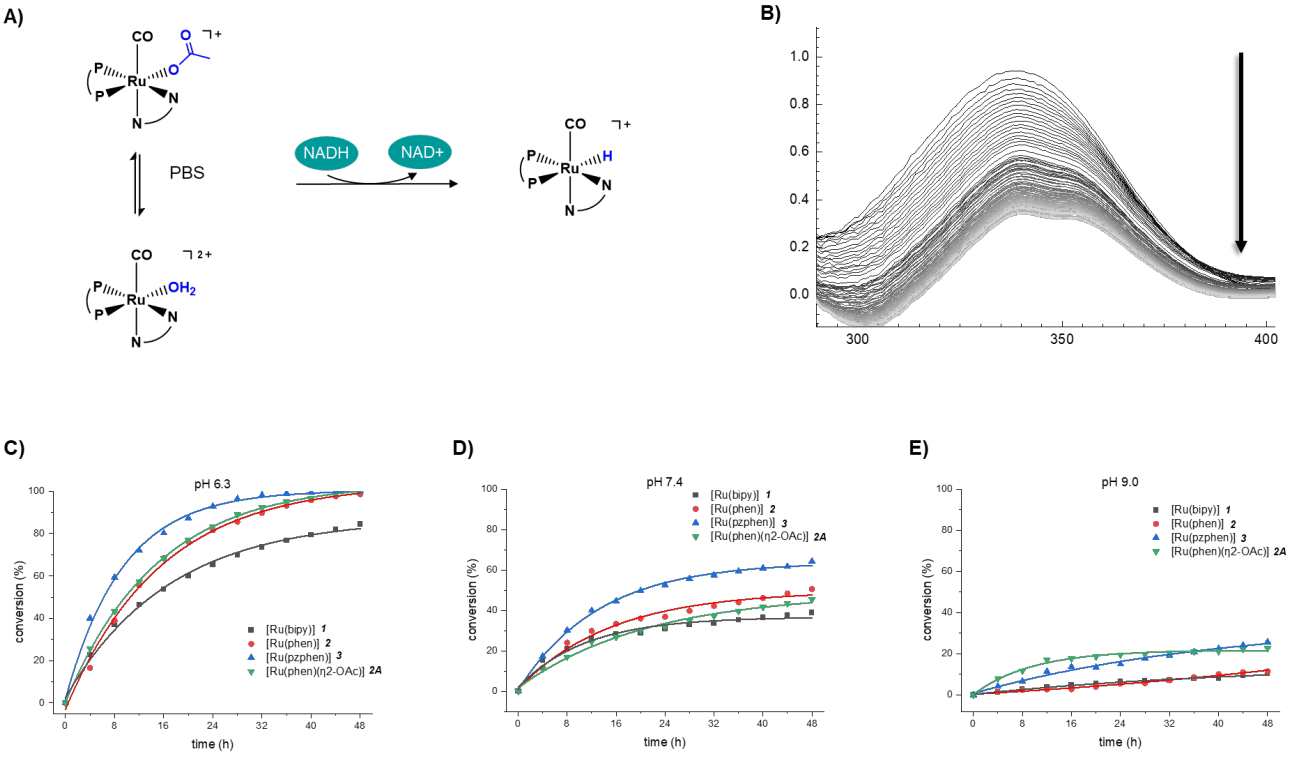

Figure 8. A) Scheme of the reaction of 1,4-NADH upon addition of complexes **1-3, 2A** and NADH in PBS buffer. B) UV-Vis absorption spectra focusing on the band at 340 nm of 1,4-NADH reacting with complex **3** (1:1 ratio) in PBS at pH 7.4 recorded over 48 hours. Plotted absorption data for the effect of pH on the stochiometric 1,4-NADH oxidation performed by complexes **1-3** and **2A**, where C) is pH 6.3, D) pH 7.4 and E) pH 9.0.

Catalytic 1,4-NADH oxidation under aerobic conditions

The monocarbonyl Ru(II) complexes **1-3** and **2A** were also investigated for the catalytic NADH oxidation reaction, using molecular oxygen as oxidizing agent (Figure 9). The reaction was carried out in deuterated PBS at both pD 7.4 and 6.3, bubbling air through 5 ml of stock solutions containing the catalysts (3.50 μmol) and NADH (17.50 μmol, 5 equiv.) (see experimental for details). The reactions were followed by ^{1}H NMR spectroscopy monitoring the formation of NAD^+ within 12 hours (Figure 9B and Figures S41-S44). Interestingly, complexes **1-3** were able to catalyse the oxidation of NADH under aerobic conditions forming NAD^+. However, again a well-defined trend based on the extension of the aromatic N^N ligand was clearly observed, highlighting an enhancement in the rate of oxidation increasing the aromaticity of the N^N ligand, in line with

the previous UV-Vis results. The effect of the pH played also a central role: a maximum of activity was observed at the most acidic pH 6.3 for all the complexes (TOF numbers ranging from 0.14 to 0.82 h^{-1}) (Figure 4D, Table 5). At pH 7.4, TOFs were found to markedly decrease and none of the catalysts reached the total conversion in 12 hours (Figure 4E), likely to be due to the already discussed differences in the hydrolysis rates of the complexes depending on the pH.

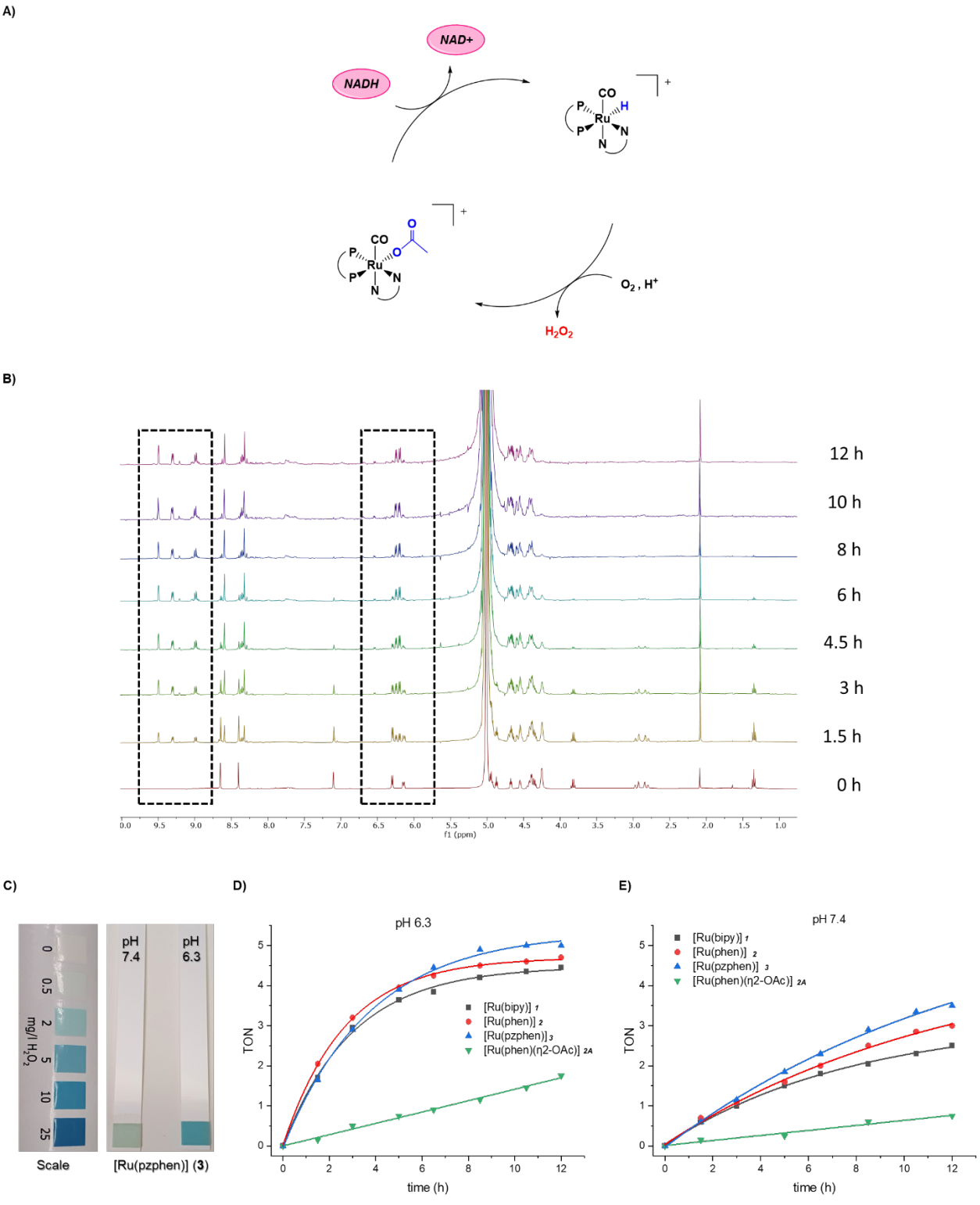

Figure 9. A) Proposed catalytic pathway for the oxidation of NADH accomplished by complexes **1-3** and **2A**. B) Stacked ^{1}H NMR kinetics of the oxidation of NADH performed by complex **3** (20%) at pH 6.3 in a time interval of 12 hours. C) Detection of H_2O_2 during the NADH reduction kinetics carried out by complex **3** at pH 6.3 and 7.4. Trends of turnover number (TON) *versus* time at pH D) 6.3 and E) 7.4.

The pyrazinophenanthroline complex **3** demonstrated to be the fastest catalyst, completing the NADH oxidation in about 10 hours at pH 6.3 with a calculated TOF number of 0.82 h^{-1}, even reacting partially in suspension after forming the hydride derivative which is only moderately water soluble. In contrast, complex **1** bearing the bipyridine system, showed the lowest conversions at both pHs, compared to the other monocarbonylated cationic complexes. Complex **2A** followed the same pH trend as the other complexes but exhibiting very scarce catalytic activity in all cases. Furthermore, as expected, **4** did not show any activity towards the NADH oxidation reaction.

Notably, after bubbling air through the solution for two hours, the formation of H_2O_2 was detected by the appearance of a blue colour on hydrogen peroxide detection sticks (Figure 9C), revealing that H_2O_2 was present in concentrations ranging from 2-10 mg/L depending on both the pH and the chemical structure of the catalyst. The development of hydrogen peroxide comes from the reduction of O_2 by the ruthenium hydride intermediate, outlining a catalytic cycle as described in Figure 9A. Nevertheless, we cannot exclude that the ruthenium hydrides react also with H^+ to produce H_2.

Table 5. Kinetic data for the regiospecific oxidation of NADH to 1,4-NAD^+ catalysed by complexes **1**-**4** (20%) and **2A** within 12 h at pD 6.3 and 7.4.

Ru(II) complex	***TOF (h^{-1})***		***TON***	
	pH 6.3	**pH 7.4**	**pH 6.3**	**pH 7.4**
*[Ru(bipy)] (**1**)*	0.67	0.32	4.45	2.5
*[Ru(phen)] (**2**)*	0.75	0.34	4.7	3.25
*[Ru(pzphen)] (**3**)*	0.82[(a)]	0.38	5[(a)]	3.6
*[Ru(phen)(η^2-OAc)] (**2A**)*	0.14	0.07	1.75	0.75

[(a)] catalytic cycle completed in *ca.* 10 hours.

Electrochemistry studies

Complexes **1-4** and **2A** show ligand field dependent activity for catalytic NAD^+ reduction (TH with formate) and NADH oxidation (reduction of O_2 to H_2O_2). Key steps of the proposed catalytic cycles involve the generation of ruthenium hydride species and the transfer of the metal hydride to substrates. Electrochemical characterization of complexes **1-4** and **2A** may therefore, help rationalizing trends in their reactivity, given that thermodynamic driving forces to accept a hydride ligand from a H-donor, and to transfer the metal-hydride to a substrate are correlated to electron density of a metal centre in its given ligand field. In seminal work, Kubiak and coworkers[46] illustrated that the hydride donor strength increases (smaller hydricity value) linearly with more

negative reduction potentials across a series of related complexes;[47] a correlation, based on established thermochemical cycles that connect hydricity and homolytic bond free energy of a metal–hydride bond.[48] Conversely, complexes with higher electron density at the metal, causing a more negative reduction potential, become worse hydride acceptors in M–H forming reactions with H–donors.

Motivated by these correlations, we determined the electrochemical reduction potentials of complexes **1-4** and **2A** as a proxy for relative trends in their hydricity (Figure 10). Due to low solubility and precipitation of charge neutral species upon electrochemical reduction in aqueous solvent, cyclic voltammetry (CV) was performed in DMF electrolyte with 0.1 M $TBAPF_6$, given that relative trends of reduction potentials for complexes **1-4** and **2A** will be similar in DMF and water. The first reduction event, which we analyse as a proxy for the relative hydricity of corresponding metal hydrides, is irreversible for all complexes except **2A**. The likely reason for this irreversibility is reductively induced dissociation of the anionic acetate ligand[49]. This loss of a donor causes an expected peak separation, measured approximately 0.5 V, between the Ru^{2+}/Ru^{+} reduction peak (with acetate still coordinated) and the corresponding Ru^{2+}/Ru^{+} oxidation peak (after loss of acetate) for complexes **2-4**. Accordingly, instead of half-wave potentials, we compare reduction peak potentials of all complexes, which we determined to be –1.80, –1.72, –1.66, –2.50, and –1.90 V for complexes **1**, **2**, **3**, **4** and **2A**, respectively. Complex **4** shows by far the most negative reduction potential, rationalized by the fact that among the presented series of compounds it is the only charge neutral species with much higher electron density at the metal center compared to cationic complexes **1-3** and **2A**. Across the cationic series **1**-**3**, the reduction potentials trend from most negative (–1.80 V for **1**) to least negative (–1.66 V for **3**) with increasing size of the N^N π-system. As expected, with –1.90 V complex **2A** possesses a more negative reduction potential than its analogue **2**, due to lack of the electron withdrawing CO ligand that reduces the electron density at the metal.

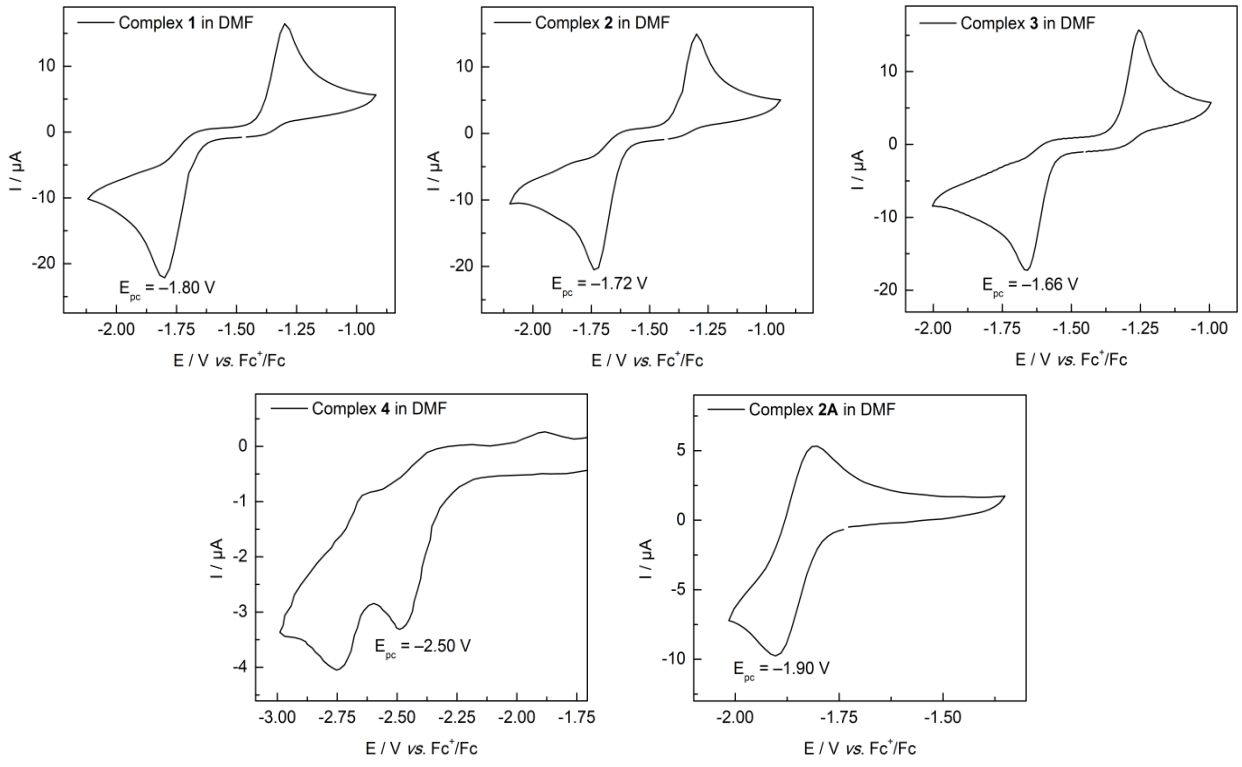

Figure 10. Cyclic voltammograms of complexes **1-4** and **2A** as indicated in the figure legends. Data was recorded in a 0.1M $TBAPF_6$ in DMF solution with a glassy carbon working-, a platinum counter- and a silver wire pseudo-reference electrode and ferrocene added for referencing.

Additionally, the most distinguishing feature in the CV of complex **2A** is that its Ru^{2+}/Ru^{+} reduction event is fully reversible, clearly demonstrating that the acetate ligand is more strongly bound in **2A**, being in a bidentate coordination, than in all other complexes of the series.

To assess thermodynamic contributions of the different ligand environments to the observed reactivity of complexes **1-4** and **2A**, the measured reduction potentials can be correlated with observed turnover frequencies NADH for oxidation and NAD^{+} reduction (Table 6 and Figure 11). For NADH oxidation, the graphical representation of plotting TOF values for NADH oxidation against reduction peak potentials (Figure 11, left), illustrates that complexes **1-3** show a clean linear trend of reduction potential and NADH oxidation TOF. The reason is that in the very comparable ligand environments, the change in reaction rate is only modulated by thermodynamic effects represented by the reduction potential, while kinetic effects remain unchanged. With increasingly negative reduction potential, the driving force to transfer a hydride from NADH to the ruthenium centre decreases, which slows down the reaction rate for NADH oxidation. A linear fit through the data points for well-comparable complexes **1-3** shows an intercept with the potential axis at –2.47 V, meaning that for all complexes in such coordination sphere with a more negative reduction potential than –2.47 V, the TOF for NADH oxidation is expected to be 0. Interestingly, this is exactly what we experimentally observed for complex **4** (reduction potential –2.50 V), which is inactive towards NADH oxidation.

Table 6. Tabulated electrochemical reduction potentials for complexes **1-4** and **2A**. TOF values for NAD^{+} hydrogenation and NADH oxidation at pH = 6.3 as given in Tables 2 and 4 are again included for convenience to support the discussion on trends in TOF and reduction potentials.

	Compound				
Entry	**1**	**2**	**3**	**4**	**2A**
E_{pc} first reduction [V vs. Fc^{+}/Fc]	–1.80	–1.72	–1.65	–2.5	–1.93
TOF of NADH oxidation [h^{-1}]	0.67	0.75	0.82	inactive	0.14
TOF of NAD+ hydrogenation [h^{-1}]	0.2	0.12	0.03	6.08	inactive

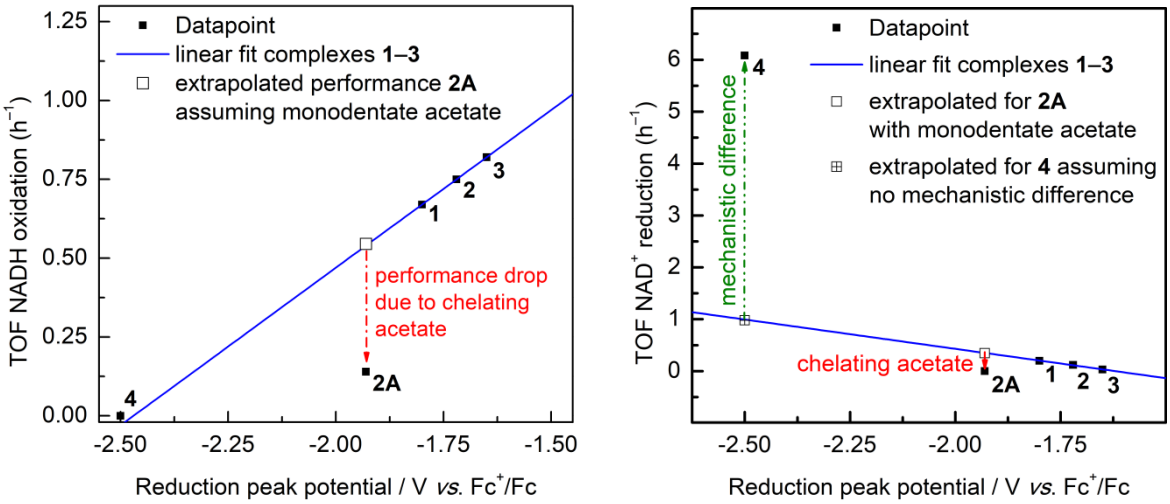

Figure 11. *Left:* Correlation of TOF for NADH oxidation with corresponding first reduction peak potential of complexes **1-4** and **2A**, illustrating the influence of different thermodynamic driving force on the observed reaction kinetics. *Right:* Correlation of TOF for NAD+ reduction with corresponding first reduction peak potential of complexes **1-4** and **2A**, illustrating influence of different thermodynamic driving force on the observed reaction kinetics. A deviation from the linear fit through the well-comparable complexes **1-3** strongly suggests additional effects beyond simple hydricity modulation for catalyst **4**.

In addition to thermodynamic effects described above, also kinetic reaction barriers can play a role for the observed TOF values, as complex **2A** clearly illustrates in the TOF *vs*. reduction potential plot (Figure 11, left). **2A** differs from the series by lack of the electron withdrawing CO ligand causing a slightly more negative reduction potential, yet **2A** drastically falls of the linear trend observed for complexes **1-4**. The considerably lower TOF of **2A** is rationalized by the fact that that with CO removed, the acetate ligand in complex **2A** is coordinated in bidentate fashion, as evidenced by XRD analysis and reversible reduction in CV (vide supra). Considering that exchange of acetate ligands is crucial to facilitating the catalytic cycle makes it obvious that the chelate effect drastically slows down this elementary step, strongly impeding catalytic turnover.

With respect to NAD^+ hydrogenation, the analogous correlation of TOF *vs*. reduction potentials yields similar results (Figure 11, right). Specifically, complexes **1-3** show an increasing TOF for NAD^+ hydrogenation with increasingly more negative reduction peak potentials. With NAD^+ hydrogenation being the reverse reaction to NADH oxidation, this inverse correlation of thermodynamic driving force (reduction potentials) and reaction rates (TOF) are just as expected. Given that extreme reduction potentials coincide with poor hydride acceptor properties of a metal complex, the trend in TOF values suggests that for NAD^+ hydrogenation with formate as the H-donor, the rate limiting step is not Ru–H generation, but the transfer of the ruthenium-hydride to the NAD^+ substrate; a reaction step that is enhanced with lower hydricity of the complexes. A linear fit through the well-comparable series **1-3** again reveals that complex **2A**, which is inactive for NAD^+ hydrogenation, suffers from lower TOF than predicted by simple thermodynamics, due to its kinetic penalty of bidentate acetate coordination. The most interesting aspect of the correlation plot, however, is observed for the picolinamidate complex **4**, which performs drastically better in NAD^+ hydrogenation than all other tested candidates of this

model study. As a quantitative measure of electron density at the metal site, the most negative reduction potential of **4** suggests that as the most electron rich species in the series, it forms the most reactive hydride with the smallest hydricity value, resulting in the highest TOF for NAD^+ hydrogenation. Yet, the experimentally observed TOF value is 6-fold higher than the prediction of trends derived from thermodynamic driving force alone. This emphasizes that for complex **4** additional kinetic and probably mechanistic changes may be induced by the picolinamidate ligand. To the best of our knowledge, the most convincing hypothesis is that picolineamide acts as a hemilabile ligand during catalytic NAD^+ hydrogenation. This situation generates possibility for two mechanistic advantages for NAD^+ hydrogenation with catalyst **4** in comparison to catalysts **1-3** and **2A**. First, as the only charge neutral complex in the series, catalyst **4** has no pronounced coulombic repulsion for the approach of cationic substrate NAD^+, which is expected to enhance the TOF for NAD^+ conversion considerably. Second, the potential hemilability of picolineamidate allows a direct coordination of NAD^+ at the reactive Ru centre, which places the required carbon atom in right proximity and geometry for an intramolecular hydride transfer from Ru to NAD^+. All other catalysts **1-3** and **2A** are restricted to an outer sphere intermolecular hydride transfer over much greater distance with less favourable geometry, potentially supported by π-π interactions of the N^N chelators with NAD^+. We like to emphasize that the presented electrochemical study highlighted that NAD^+ hydrogenation with catalyst **4** is likely to follow a reaction mechanism that is different to the one for NAD^+ hydrogenation with catalysts **1-3** and **2A**. The provided explanation merely represent a plausible hypothesis that cannot be validated entirely by the experimental data available, which set the stage for a detailed quantum chemical analysis of the situation that has further confirmed our description as presented in the following.

Antiproliferative activity

The antiproliferative activity of the Ru(II) complexes **1-3** was studied in a small panel of human cancer cells *in vitro* (see experimental for details). After 72 h incubation, the compounds display moderate to high cytotoxicity in cancer cells, with EC_{50} values ranging from 0.71 to 15.5 μM (Table 7), with the most active Ru(II) monocarbonyl complex being derivative **1** (e.g. EC_{50} = 0.71 μM in MCF7 cells). The latter is also the least active in non-tumorigenic VERO cells showing a good selectivity (selectivity index = 13.5). Notably, all the compounds, except for **2A** (with EC_{50} values between 10-20 μM), are more potent than cisplatin in all cell lines, with complex **1** being ca. 35-fold more active than cisplatin. These data suggest that this class of complexes can overcome the resistance to cisplatin.

Table 7. Antiproliferative activity (EC_{50} values) of complexes **1-3**, **2A** and cisplatin against human breast cancer (MCF-7), hormone-independent breast cancer (MDA), human lung adenocarcinoma (A549), human colon cancer (HT29), and healthy cells derived from the kidney of an African green monkey (VERO). The compounds were incubated for 72 h. Range of selectivity index (SI) towards the respective cancer cells calculated as [EC_{50} VERO/EC_{50} cancer cell line]; (n = 3).

Compound	EC_{50} (μM)					SI
	MCF-7	MDA-MB-231	A549	HT29	VERO	
*[Ru(bipy)] (**1**)*	0.71 ± 0.13	1.03 ± 0.13	1.1 ± 0.1	1.3 ± 0.09	9.59 ± 0.33	13.5-7.4
*[Ru(phen)] (**2**)*	1.47 ± 0.06	1.06 ± 0.26	1.84 ± 0.15	0.98 ± 0.05	3.34 ± 0.14	3.4-2.3
*[Ru(pzphen)] (**3**)*	1.26 ± 0.09	1.46 ± 0.15	1.71 ± 0.13	1.64 ± 0.08	3.12 ± 0.13	2.5-1.8

[Ru(η²-OAc)] (**2A**)	15.53 ± 0.95	14.57 ± 0.77	10.53 ± 0.59	9.72 ± 0.21	22.09 ± 0.83	2.3-1.4
Cisplatin	**26.1 ± 0.6**	**11.7 ± 1.8**	**3.47 ± 0.13**	**7.99 ± 1.38**	**12.2 ± 1.4**	**3.5-0.5**

ROS production

We investigated whether the catalytic Ru(II) complexes **1-3** can induce a high level of reactive oxygen species (ROS) in human cancer and non-tumorigenic cells after 2 hours treatment. The obtained results are shown in Figure 12 and reveal that all the compounds can significantly increase ROS production in cancer and VERO cells, although to a lesser extent than H_2O_2 treatment.

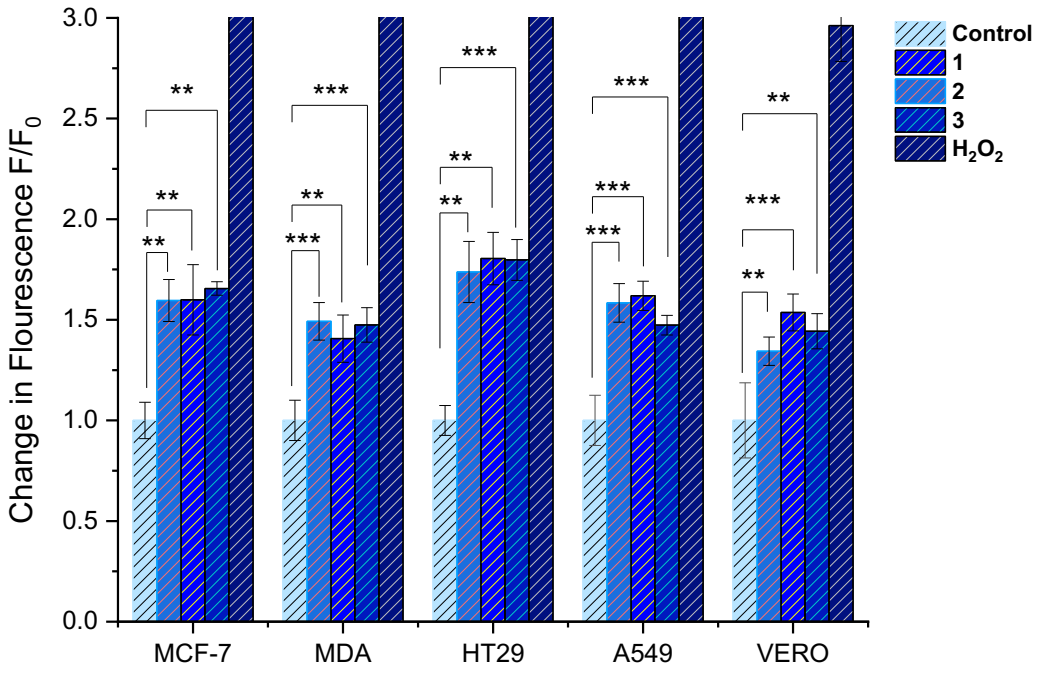

Figure 12. Induction of H_2O_2 production by complexes **1**-**3** (50 μM) after 2 h incubation in MCF-7, MDA-MB-231, A549, HT29 and VERO cell lines. The histograms show the change in fluorescence measured using CM-H_2DCFDA fluorescent probe with respect to the control (untreated cells) and the treatment with H_2O_2.

Intracellular transfer hydrogenation catalysis

To demonstrate the catalytic activity of the ruthenium complexes **1-3** in biological environment, we followed an already reported strategy by Do *et al.* [50] based on fluorescence microscopy in living cells. In detail, an aldehyde-containing probe molecule (BODIPY-CHO) was synthesized that would exhibit fluorescence emission upon reduction to its alcohol form (BODIPY-OH). This reaction might be catalysed by the Ru(II) complexes in the presence of an endogenous hydride source, such as NADH (Figure 13A). The expected product BODIPY-OH has an excitation wavelength in the visible region (480 nm) and its emission is measured at 530 nm. Before treating the cancer cell lines with the probe and the Ru(II) complexes, the reaction was monitored in a cuvette by fluorescence spectrophotometry over time. The obtained results show that the all the Ru catalysts **1-3** can mediate the reaction of BODIPY-CHO (5 equiv.) with NADH (5 equiv.) in a solution of ^{t}BuOH/H_2O (1:4), leading

to a ca. 12-fold increase in fluorescence emission at 530 nm during 24 hours, due to the formation of BODIPY-OH (Figures 13B and S45).

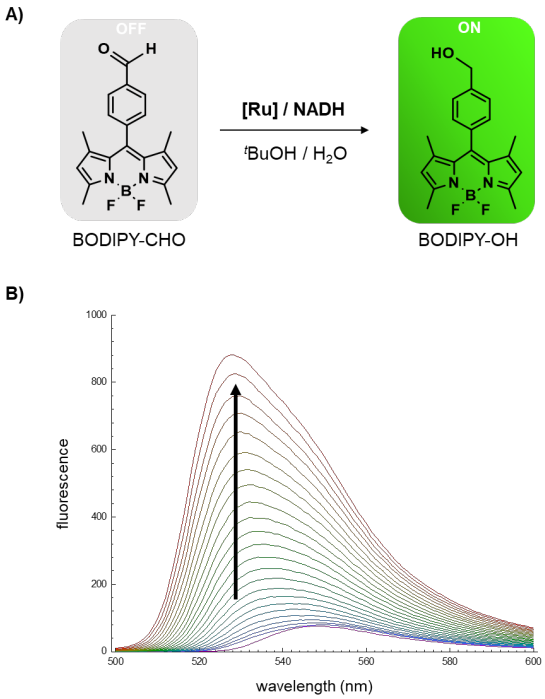

Figure 12. A) Proposed reaction for the reduction of the aldehyde probe BODIPY-CHO in presence of the Ru(II) catalysts **1-3** and NADH as hydride source. B) Fluorescence spectra (λ_{exc} = 480 nm) obtained from the reaction of BODIPY-CHO and NADH in the presence of [Ru(pzphen)] (**3**) in ^{t}BuOH / H_2O (1 : 4) at room temperature in aerobic conditions. The spectral changes were recorded at different time intervals within 24 h.

Afterwards, the same reaction was monitored in human cancer cells by fluorescence microscopy. Live cell images of MDA-MB-231 cells are reported in Figure 14, whereby the cells were incubated with 30 μM of BODIPY-CHO for 4 hours, washed with fresh media and then exposed to complexes **1-3** (20 μM) for 2 hours. Results are presented in comparison to cells treated with the non-fluorescent BODIPY-CHO and with benchmark fluorescent BODIPY-OH. The relative integrated fluorescence intensities of the cell images were quantified using the program ImageJ and reported as the fold-change relative to that of the BODIPY-CHO (Figure 14A). Cells that were treated with the latter showed weak fluorescence, whereas cells that were treated with BODIPY-OH showed more intense fluorescence. The obtained results show that all the compounds develop comparable fluorescence emission intracellularly over time, and further corroborate the hypothesis of intracellular catalytic reactivity of the Ru(II) complexes via transfer hydrogenation.

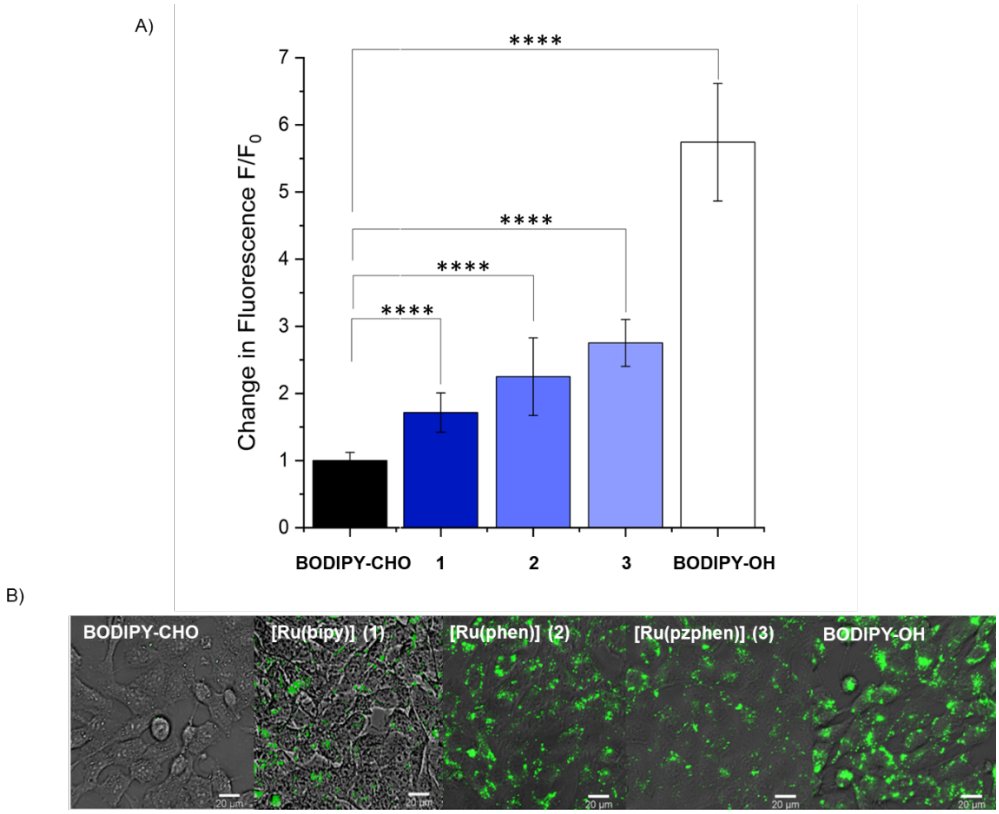

Figure 14. A) The plot shows the change in fluorescence of live MDA-MB-231 cells after treatment with complexes **1**-**3** (20 μM) for 2 h. The fold-changes are relative to that observed in the BODIPY-CHO only treated cells. The error bars show the standard deviation from the mean. B) Inverted light microscope images of MDA-MB-231 cells treated with BODIPY-CHO, complexes **1**-**3** and BODIPY-OH (20 μM).

In order to assess the ability of the Ru(II) catalysis to interact with NADH and form hydride species in cellular environment, cell extracts of human MCF-7 breast cancer cells were treated with the most active complex **2** towards NADH oxidation. Thus, freshly prepared cell extracts were treated with **3** (2 mM) in PBS pD 7.4 for 24 hours. In this time frame, we could observe the formation of a cloudy precipitate at the bottom of the tube (Figure 15A). The solution was carefully removed and the precipitate dissolved in deuterated methanol to record ^{1}H NMR and ^{31}P NMR spectra (Figure 15 and S46). The results showed the appearance of the typical doublet of doublets at -6.1 ppm (Figure 15B), which was attributed to the formation of the ruthenium hydride derivative (**2H**). Despite the promising results, we do not exclude also the formation of other adducts of the Ru(II) complex with different biomolecules.

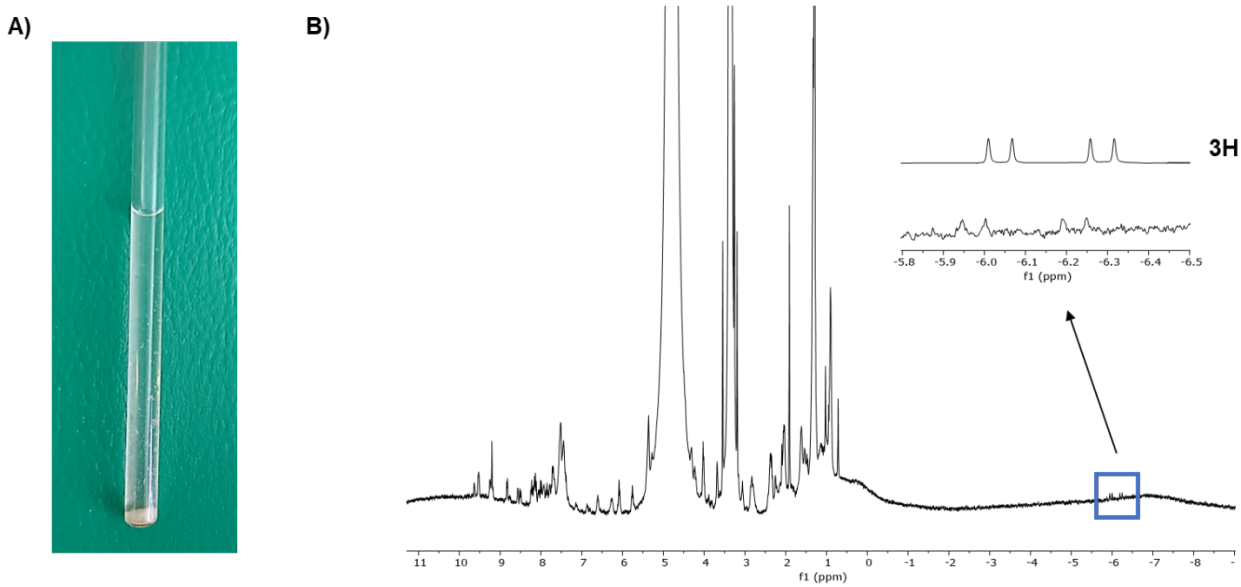

Figure 15. A) Precipitate formation after incubation of MCF-7 cancer cell extracts for 24 h with a 0.2 mM solution of complex **3** in deuterated PBS pD 7.4. B) ^{1}H NMR spectrum in CD_3OD of the precipitate obtained after incubating the cancer cell extracts with complex **3** for 24 h. Inset shows the comparison between the formed **3H** in the cell extracts and the same synthetically isolated compound.

Conclusions

The special ability of organometallic complexes to catalyse various transformations might offer new effective mechanisms for the treatment of cancer. The NAD^+/NADH redox couple has recently emerged as the new target for next-generation catalytic anticancer metallodrugs. Because of the vital role of these coenzymes in mitochondrial electron transport chain, cell metabolism, enzymatic reactions and several other biochemical pathways, changes in the intracellular NAD^+/NADH ratio via transfer hydrogenation catalysed by TM complexes can eventually lead to cell death. While most of the organometallic drugs shown to perform TH in cells feature metal-arene moieties[7], we have reported here on a different family of water-soluble organometallic TH catalysts based on a Ru(II) monocarbonyl scaffold.

Together, insight from the kinetic and electrochemical characterization suggests that for catalytic NADH oxidation (eventually leading also to H_2O_2 formation), the rate limiting step is the hydride transfer from 1,4-NADH to the Ru(II) complexes, whereas for NAD^+ hydrogenation with formate as the hydride donor, the rate limiting step may be the transfer of the ruthenium hydride to the NAD^+ substrate. The latter is further modulated by the presence of di-cationic aquo- or mono-cationic hydroxo-species in the cases of complexes **1-3** subjected to hydrolysis processes, at variance with compound **4**. It is worth mentioning that preliminary DFT calculations also confirm the energetically unfavourable hydride formation, in line with other studies on the reactivity of metal-arene complexes toward hydride transfer reactions associated with NADH regeneration [2, 3].

Complex **4** resulted to be the best catalyst of the series (ca. 46-fold more active) in NAD^+ reduction using formate, and overall endowed with a different TH mechanism with respect to the other complexes. Comparing the performance of complex **2A** to the rest of the series revealed that a kinetic labilisation of the acetate ligands is crucial for good catalyst performance beyond simple thermodynamic considerations. While these correlations of electrochemical and kinetic data allow a reasonable qualitative hypothesis about reaction

pathways and reaction barriers, they cannot serve as absolute proof–and further studies are necessary to elucidate the mechanisms of catalysis for this family of organometallic compounds.

Preliminary studies on the antiproliferative effects of complexes **1-3** showed that the compounds are particularly active towards human cancer cells with respect to non-tumorigenic ones. Most notably, the compounds can promote the TH reaction on a fluorogenic substrate in living cells, and Ru(II) hydride formation has been detected by incubation of complex **3** with cancer cell extracts by ^{1}H NMR spectroscopy.

Overall, our study provides evidence for the applicability of Ru(II) monocarbonyl complexes for TH catalysis in cellular environment, evidencing the power of organometallic chemistry, beyond metal-arene compounds, for the design of highly versatile and water-compatible catalytic metallodrugs.

Experimental section

Synthesis of [Ru(OAc)(CO)(dppb)(bipy)]OAc (1)

[Ru(η^1-OAc)(η^2-OAc)(dppb)(CO)] (50.0 mg, 0.074 mmol) and 2,2'-bipyridine (bipy) (11.5 mg, 0.074 mmol) were dissolved in 1.5 mL of methanol and the mixture was stirred at 60 °C overnight. The solvent was evaporated under reduced pressure and the product was dissolved in 0.5 mL of dichloromethane. Addition of 5 mL of diethyl ether afforded a yellow precipitate, which was filtered and dried under reduced pressure. Yield: 50 mg (80 %). Elemental analysis calcd (%) for $C_{43}H_{42}N_2O_5P_2Ru$: C 62.24, H 5.10, N 3.38; found: C 62.26, H 5.13, N 3.40. ^{1}H NMR (400.1 MHz, CD_3OD, 298 K): δ = 9.17 (br t, $^3J_{HH}$ = 3.3 Hz, 1H; bipy), 8.57 (d, $^3J_{HH}$ = 5.5 Hz, 1H; bipy), 8.24 (d, $^3J_{HH}$ = 6.8 Hz, 1H; bipy), 8.13 (m, 4H; bipy), 7.95 (td, $^3J_{HH}$ = 7.8 Hz, $^4J_{HH}$ = 1.6 Hz, 1H; bipy), 7.72-7.32 (m, 17H; Ph), 7.09 (t, $^3J_{HH}$ = 7.0 Hz, 1H; Ph), 6.83 (td, $^3J_{HH}$ = 8.1 Hz, $^4J_{HH}$ = 2.4 Hz, 2H; Ph), 6.46 (t, $^3J_{HH}$ = 8.8 Hz, 2H; Ph), 3.16 (m, 2H; PCH_2), 2.94-2.72 (br m, 2H; PCH_2), 2.27-1.93 (m, 4H; CH_2), 1.91 (s, 3H; CH_3), 1.59 (s, 3H; CH_3). ^{31}P{^{1}H} NMR (162.0 MHz, CD_3OD, 298 K): δ = 31.2 (d, $^2J_{PP}$ = 24.5 Hz), 29.2 ppm (d, $^2J_{PP}$ = 24.5 Hz).

Synthesis of [Ru(OAc)(CO)(dppb)(pz-phen)]OAc (3)

Complex **3** was prepared following the procedure described for **1**, using pyrazino[2,3-*f*][1,10]phenanthroline (PzPhen) (17.5 mg, 0.074 mmol) in place of bipyridine. Yield: 60 mg (89%). Elemental analysis calcd (%) for $C_{47}H_{42}N_4O_5P_2Ru$: C 62.32, H 4.67, N 6.18; found: C 62.18, H 4.55, N 6.07. ^{1}H NMR (400.1 MHz, $CDCl_3$, 298 K): δ = 9.68 (br t, $^3J_{HH}$ = 3.3 Hz, 1H; PzPhen), 9.63 (d, $^3J_{HH}$ = 8.1 Hz, 1H; PzPhen), 9.41 (d, $^3J_{HH}$ = 8.0 Hz, 1H; PzPhen), 9.19-9.06 (m, 3H; PzPhen), 8.16 (m, 3H; Ph), 7.76 (dd, $^3J_{HH}$ = 8.1 Hz, $^4J_{HH}$ = 5.4 Hz, 1H; PzPhen), 7.66-7.35 (m, 13H; Ph), 6.44-6.20 (m, 5H; Ph), 3.47 (m, 1H; PCH_2), 3.29 (br t, 1H; PCH_2), 3.10 (m, 1H; PCH_2), 2.63 (br t, 1H; PCH_2), 2.37-2.04 (m, 3H; CH_2), 1.99 (s, 3H; CH_3), 1.54 (m, 1H; CH_2), 1.50 ppm (s, 3H; CH_3). ^{13}C{^{1}H} NMR (100.6 MHz, $CDCl_3$, 298 K): δ = 204.1 (t, $^2J_{CP}$ = 15.0 Hz; CO), 177.2 (s; *C*OCH_3), 176.5 (s; *C*OCH_3), 157.7-124.9 (m; aromatic carbon atoms), 28.6 (d, $^1J_{CP}$ = 26.9 Hz; P*C*H_2), 25.1 (d, $^1J_{CP}$ = 30.6 Hz; P*C*H_2), 25.1 (s; CO*C*H_3), 24.1 (s; CH_2), 23.9 (d, $^4J_{CP}$ = 3.6 Hz; CO*C*H_3), 21.7 ppm (d, $^2J_{CP}$ = 3.4 Hz; CH_2). ^{31}P{^{1}H} NMR (162.0 MHz, $CDCl_3$, 298 K): δ = 31.7 (d, $^2J_{PP}$ = 23.5 Hz), 29.6 ppm (d, $^2J_{PP}$ = 23.5 Hz).

Synthesis of [Ru(OAc)(CO)(dppb)(pica)] (4)

[Ru(η^1-OAc)(η^2-OAc)(dppb)(CO)] (50.0 mg, 0.074 mmol) and picolinamidate (pica) (9.1 mg, 0.074 mmol) were dissolved in 1.5 mL of ethanol and the mixture was stirred at 75 °C overnight. The solvent was evaporated under reduced pressure and the product was dissolved in 0.5 mL of dichloromethane. Addition of 5 mL of diethyl ether afforded a yellow precipitate, which was filtered and dried under reduced pressure. Yield: 37 mg mg (67 %). Elemental analysis calcd (%) for $C_{37}H_{36}N_2O_4P_2Ru$: C 60.40, H 4.93, N 3.81; found: C 60.37, H 4.95, N 3.80. ^{1}H NMR (400.1 MHz, CD_3OD, 298 K): δ = 8.39 (br t, $^3J_{HH}$ = 3.6 Hz, 1H; pica), 7.93 (d, $^3J_{HH}$ = 7.8 Hz, 1H; pica), 7.81 (t, $^3J_{HH}$ = 8.7 Hz, 2H; pica), 7.64 (m, 5H; Ph), 7.53-7.24 (m, 10H; Ph), 7.14 (t, $^3J_{HH}$ = 7.9 Hz, 1H; Ph), 7.04 (t, $^3J_{HH}$ = 6.5 Hz, 2H; Ph), 6.95 (m, 2H; Ph), 5.32 (s, 1H, NH), 3.15 (m, 2H; PCH_2), 2.99 (m, 2H; PCH_2), 2.33 (m, 1H; PCH_2), 1.65 (m, 2H, CH_2), 1.50 (s, 3H; CH_3), 1.35 (m, 2H; CH_2). ^{13}C{^{1}H} NMR (100.6 MHz, CD_3OD, 298 K): δ = 205.2 (d, $^2J_{CP}$ = 15.1 Hz; CO), 178.9 (s; *C*OCH_3), 173.3 (s; CONH) 154.6-123.6 (m; aromatic carbon atoms), 32.3 (s; *C*H_2), 26.6 (s; *C*H_2), 21.1 (s; *C*H_2), 20.8 (s; CH_2). ^{31}P{^{1}H} NMR (162.0 MHz, CD_3OD, 298 K): δ = 40.1 (d, $^2J_{PP}$ = 30.3 Hz), 36.7 ppm (d, $^2J_{PP}$ = 30.3 Hz).

Synthesis of [Ru(OAc)(dppb)(phen)]OAc (2A)

[Ru(η^2-OAc)$_2$(dppb)] (50.0 mg, 0.077 mmol) and 1,10-phenanthroline (14.0 mg, 0.077 mmol) were dissolved in 1.5 mL of methanol and the mixture was stirred at 60 °C overnight. The solvent was evaporated under reduced pressure and the product was dissolved in 0.5 mL of dichloromethane. Addition of 5 mL of diethyl ether afforded a yellow precipitate, which was filtered and dried under reduced pressure. Yield: 56 mg (88%). Elemental analysis calcd (%) for $C_{44}H_{42}N_2O_4P_2Ru$: C 63.99, H 5.13, N 3.39; found: C 63.59, H 4.80, N 3.27. ^{1}H NMR (400.1 MHz, CD_2Cl_2, 298 K): δ = 8.97 (ddd, $^3J_{HH}$ = 5.1 Hz, $^4J_{HH}$ = 2.3 Hz, $^6J_{HH}$ = 1.3 Hz, 1H; phen), 8.46-8.39 (m, 2H; phen), 8.37 (dd, $^3J_{HH}$ = 8.2 Hz, $^4J_{HH}$ = 1.3 Hz, 1H; phen), 8.00-7.85 (m, 6H; aromatic protons), 7.78 (ddd, $^3J_{HH}$ = 8.0 Hz, 4J_{HH} = 5.2 Hz, 6J_{HH} = 0.7 Hz, 1H; phen), 7.73-7.58 (m, 4H; aromatic protons), 7.50 (td, $^3J_{HH}$ = 7.7 Hz, $^4J_{HH}$ = 1.8 Hz, 2H; Ph), 7.45-7.24 (m, 6H; Ph), 6.59 (tq, $^3J_{HH}$ = 7.4 Hz, $^4J_{HH}$ = 1.1 Hz, 1H; Ph), 6.27 (td, $^3J_{HH}$ = 8.3 Hz, $^4J_{HH}$ = 2.2 Hz, 2H; Ph), 5.58 (t, $^3J_{HH}$ = 8.5 Hz, 2H; Ph), 3.23 (m, 1H; PCH_2), 2.67 (m, 1H; PCH_2), 2.41 (m, 2H; PCH_2), 2.20 (m, 2H; CH_2), 1.97 (m, 1H; CH_2), 1.87 (s, 3H; CH_3), 1.66 (m, 1H; CH_2), 1.17 ppm (s, 3H; CH_3). ^{13}C{^{1}H} NMR (100.6 MHz, CD_2Cl_2, 298 K): δ = 189.1 (s; $COCH_3$), 176.4 (s; $COCH_3$), 159.7-124.1 (m; aromatic carbon atoms), 29.2 (d, $^1J_{CP}$ = 26.7 Hz; PCH_2), 26.9 (d, $^1J_{CP}$ = 28.1 Hz; PCH_2), 25.0 (s; CH_2), 24.3 (s; $COCH_3$), 23.7 (s; $COCH_3$), 22.5 ppm (s; CH_2). ^{31}P{^{1}H} NMR (162.0 MHz, CD_2Cl_2, 298 K): δ = 48.9 (d, $^2J_{PP}$ = 33.6 Hz), 47.8 ppm (d, $^2J_{PP}$ = 33.6 Hz).

Synthesis of hydride [Ru(H)(CO)(dppb)(NN)]PF_6 complexes (1H-3H)

[Ru(OAc)(CO)(dppb)(NN)]OAc and 1,4-NADH (1.5 equiv.) or formic acid (3 equiv.) were dissolved in 5 mL of PBS pH 7.4 and the mixture was stirred at 38 °C overnight. $NaPF_6$ (6 equiv.) was added and the resulting solution was cooled to 0 °C in order to precipitate the product as a yellow solid, which was filtered and washed with cold water (2 x 2 ml), diethyl ether (2 x 2 ml) and finally dried under reduced pressure.

[Ru(H)(CO)(dppb)(bipy)]PF_6 (1H): [Ru(OAc)(CO)(dppb)(bipy)]OAc (**1**) (25.0 mg, 0.030 mmol), 1,4-NADH (21.3 mg, 0.045 mmol) or formic acid (3.4 µL, 0.090 mmol). Yield (for formate reaction): 15.0 mg (58%). Elemental analysis calcd (%) for $C_{39}H_{37}F_6N_2OP_3Ru$: C 54.61, H 4.35, N 3.27; found: C 54.57, H 4.29, N 3.22. ^{1}H NMR (400 MHz, CD_3OD, 298 K) δ = 9.13 (s, 1H; bipy), 8.15 - 7.91 (m, 7H; bipy), 7.92 - 7.78 (m, 3H; Ph), 7.74 - 7.57 (m, 2H; Ph), 7.56 - 7.44 (m, 4H; Ph), 7.44 - 7.28 (m, 5H; Ph), 7.14 (t, $^3J_{HH}$ = 6.1 Hz, 1H; Ph), 6.96 (t, $^3J_{HH}$ = 7.4 Hz, 1H; Ph), 6.59 (t, $^3J_{HH}$ = 6.8 Hz, 1H; Ph), 6.00 (t, $^3J_{HH}$ = 8.1 Hz, 2H; Ph), 2.81 - 2.66 (m, 2H; CH_2), 2.51 - 2.16 (m, 2H; CH_2), 1.61 (s, 1H; CH_2), 1.28 (d, $^3J_{HH}$ = 15.1 Hz, 2H; CH_2), -6.33 ppm (dd, $^2J_{HP}$ = 100.6, $^2J_{HP}$ =23.6 Hz, 1H; RuH). ^{31}P{^{1}H} NMR (162 MHz, CD_3OD, 298 K) δ (ppm): 57.7 (d, $^2J_{PP}$ = 9.78 Hz), 9.5 (s), -144.5 (sept).

[Ru(H)(CO)(dppb)(phen)]PF_6 (2H): [Ru(OAc)(CO)(dppb)(phen)]OAc (**2**) (20.0 mg, 0.023 mmol), 1,4-NADH (16.6 mg, 0.035 mmol) or formic acid (2.6 µL, 0.069 mmol). Yield (for formate reaction): 15.0 mg (74%). Elemental analysis calcd (%) for $C_{41}H_{37}F_6N_2OP_3Ru$: C 55.85, H 4.23, N 3.18; found: C 55.82, H 4.24, N 3.15. ^{1}H NMR (400.1 MHz, CD_3OD, 298 K): δ = 9.51 (ddt, $^3J_{HH}$ = 4.0 Hz, $^4J_{HH}$ = 2.9 Hz, $^5J_{HH}$ = 1.5 Hz, 1H; phen), 8.51 (dd, $^3J_{HH}$ = 8.2 Hz, $^4J_{HH}$ = 3.4 Hz, 2H; phen), 8.47 (dd, $^3J_{HH}$ = 5.2 Hz, $^4J_{HH}$ = 1.6 Hz, 1H; phen), 8.11 (t, $^3J_{HH}$ = 8.5 Hz, 2H; phen), 7.90 (d, $^3J_{HH}$ = 2.2 Hz, 2H; phen), 7.85 (m, 2H; Ph), 7.72 (m, 2H; Ph), 7.62-7.00 (m, 11H; Ph), 6.47 (td, $^3J_{HH}$ = 7.5 Hz, $^4J_{HH}$ = 1.3 Hz, 1H; Ph), 6.16 (td, $^3J_{HH}$ = 7.9 Hz, $^4J_{HH}$ = 2.3 Hz, 2H; Ph), 5.70 (td, $^3J_{HH}$ = 8.5 Hz, $^4J_{HH}$ = 1.4 Hz, 2H; Ph), 3.54-3.40 (m, 2H; PCH_2), 2.83 (br m, 2H; PCH_2), 2.42-2.25 (m, 2H; CH_2), 1.62 (br m, 2H; CH_2), -6.12 ppm (dd, $^2J_{HP}$ = 99.1 Hz, $^2J_{HP}$ = 22.3 Hz, 1H; RuH). ^{13}C{^{1}H} NMR (100.6 MHz,

CD_3OD, 298 K): δ = 206.8 (dd, $^2J_{CP}$ = 17.5 Hz, $^2J_{CP}$ = 7.2 Hz; CO), 154.7-124.3 (m; aromatic carbon atoms), 23.1 (s; CH_2), 23.4 (d, $^1J_{CP}$ = 19.1 Hz; PCH_2), 21.1 (d, $^1J_{CP}$ = 24.6 Hz; PCH_2), 20.7 (s; CH_2). $^{31}P\{^1H\}$ NMR (162.0 MHz, CD_3OD, 298 K): δ = 57.4 (d, $^2J_{PP}$ = 9.8 Hz), 9.9 (br t, $^2J_{PP}$ = 9.5 Hz), - 144.7 ppm (sept, $^1J_{PF}$ = 706.5 Hz). **[Ru(H)(CO)(dppb)(pzphen)]PF_6 (3H):** [Ru(OAc)(CO)(dppb)(pzphen)]OAc (**3**) (20 mg, 0.021 mmol), 1,4-NADH (15.2 mg, 0.031 mmol) or formic acid (2.4 µL, 0.063 mmol). Yield (for formate reaction): 14.0 mg (71%). Elemental analysis calcd (%) for $C_{43}H_{37}F_6N_4OP_3Ru$: C 55.31, H 3.99, N 6.00; found: C 55.26, H 3.91, N 5.97. ^1H NMR (400.1 MHz, CD_3OD, 298 K): δ = 9.64 (br s, 1H; pzphen), 9.54 (d, $^3J_{HH}$ = 8.2 Hz, 2H; pzphen), 9.17 (s, 2H; pzphen), 8.59 (d, $^3J_{HH}$ = 4.5 Hz, 1H; pzphen), 8.17 (t, $^3J_{HH}$ = 8.6 Hz, 2H; Ph), 8.02 (dd, $^3J_{HH}$ = 8.3 Hz, $^4J_{HH}$ = 5.3 Hz, 1H; pzphen), 7.88 (t, $^3J_{HH}$ = 8.9 Hz, 2H; Ph), 7.73 (m, 2H; Ph), 7.68 (dd, $^3J_{HH}$ = 8.2 Hz, $^4J_{HH}$ = 5.4 Hz, 1H; pzphen), 7.60-7.32 (m, 8H; Ph), 6.08 (m, 3H; Ph), 5.77 (t, $^3J_{HH}$ = 7.5 Hz, 2H; Ph), 3.52 (m, 2H; PCH_2), 2.86 (br m, 2H; PCH_2), 2.37 (br m, 2H; CH_2), 1.62 (br m, 2H; CH_2), -6.06 ppm (dd, $^2J_{HP}$ = 98.3 Hz, $^2J_{HP}$ = 23.7 Hz, 1H; RuH). $^{31}P\{^1H\}$ NMR (162.0 MHz, CD_3OD, 298 K): δ = 57.7 (d, $^2J_{PP}$ = 10.8 Hz), 9.7 (s), - 144.6 ppm (sept, $^1J_{PF}$ = 707.2 Hz).

X-ray Crystallography. Crystals suitable for X-Ray measurements were obtained by slow diffusion of diethylether in DCM saturated solutions in which the ruthenium complexes were dissolved. Data were collected on a Bruker D8 Venture single crystal X-ray diffractometer equipped with a CPAD detector (Bruker Photon II), an IMS micro source with MoK_α radiation (λ = 0.71073 Å) and a Helios optic or a CMOS detector (Bruker Photon-100), a TXS rotating anode with MoK_α radiation and a Helios optic using the APEX3 software package.[51] Measurements were performed on single crystals coated with perfluorinated ether. The crystals were fixed on top of a kapton micro sampler and frozen under a stream of cold nitrogen. A matrix scan was used to determine the initial lattice parameters. Reflections were corrected for Lorentz and polarisation effects, scan speed, and background using SAINT.[52] Absorption correction, including odd and even ordered spherical harmonics was performed using SADABS.[52] Space group assignments were based upon systematic absences, E statistics, and successful refinement of the structures. The structures were solved using SHELXT with the aid of successive difference Fourier maps, and were refined against all data using SHELXL in conjunction with SHELXLE.[53, 54] Hydrogen atoms (except hydrides) were calculated in ideal positions as follows: Methyl hydrogen atoms were refined as part of rigid rotating groups, with a C–H distance of 0.98 Å and $U_{iso(H)}$ = 1.5·$U_{eq(C)}$. Non-methyl hydrogen atoms were placed in calculated positions and refined using a riding model, with methylene and aromatic C–H distances of 0.99 Å and 0.95 Å, respectively, and other C–H distances of 1.00 Å, all with $U_{iso(H)}$ = 1.2·$U_{eq(C)}$. Non-hydrogen atoms were refined with anisotropic displacement parameters. Full-matrix least-squares refinements were carried out by minimizing $\Sigma w(F_o^2 - F_c^2)^2$ with the SHELXL weighting scheme.[53, 55] Neutral atom scattering factors for all atoms and anomalous dispersion corrections for the non-hydrogen atoms were taken from *International Tables for Crystallography*.[56] The unit cells of **1** and **4** contain 4 disordered methanol molecules and 4 disordered water molecules, respectively, which were treated as a diffuse contribution to the overall scattering without specific atom positions using the PLATON/SQUEEZE procedure.[57] Images of the crystal structures were generated with Mercury.[58] CCDC XYZ-XYZ contains the supplementary crystallographic data for this paper. These data are provided free of charge by The Cambridge Crystallographic Data Centre.

Calculation of pK_a values. The determination of pKa values was performed in D_2O unbuffered solutions adjusting the pH with diluted NaOH or acetic acid solutions in the rage 4-11. The pH titration curves were fitted to the Henderson-Hasselbalch equation using the program OriginPro 2021. The errors in pKa values are estimated to be ca. ± 0.08 unit.

Catalytic NAD^+ hydrogenation. 6.25 μmol of each complex and 62.5 μmol of NAD^+ were dissolved in 1.5 ml of deuterated PBS at pD 7.3. Right before starting the ^{1}H-NMR kinetics, 312.5 μmol of formic acid were added and 0.5 ml of the solution transferred into a 5 mm NMR tube. The experiments were recorded every two hours up to 24 h, and after 36 and 48 h at 298 K. No reaction took place in the absence of the catalysts.

Catalytic pyruvate hydrogenation. For the catalytic reduction of pyruvate to lactate, 6.25 μmol of each Ru(II) complex and 62.5 μmol of pyruvate were dissolved in 1.5 ml of deuterated PBS at pD 7.3. Right before starting the ^{1}H-NMR kinetics, 312.5 μmol of formic acid were added and 0.5 ml of the solution transferred into a 5 mm NMR tube. The spectra were recorded every 8 hours up to 48 hours at 298 K. No reactions took place in the absence of the catalysts in these experimental conditions.

NADH dehydrogenation followed by UV-Vis spectrophotometry. NADH dehydrogenation reactions were performed dissolving 0.58 μmol of both 1,4-NADH and complexes **1**-**3** in 3 mL of 0.2 M phosphate buffer solution (PBS), giving a final concentration of 0.2 mM. Each experiment was acquired during a 48 h scanning kinetics at three different pHs, namely 6.3, 7.4 and 9.

Catalytic NADH dehydrogenation. Catalytic NADH dehydrogenation reactions were conducted in 0.2 M deuterated PBS at two different pD values (6.3 and 7.4). NADH oxidation experiments were carried out in a 10 ml vials dissolving 12.5 mg (17.5 μmol) of 1,4-NADH disodium salt in 5 ml of deuterated PBS. After the addition of 3.5 μmol (0.2 equiv.) of each ruthenium complex, air was bubbled into the solution by means of a laboratory pump (Laboport N96) for 12 hours with a flow rate of 1.5 ± 10% L/min. The formation of H_2O_2 was detected by Quantofix peroxide test sticks. The experiments were followed by ^{1}H-NMR at different time intervals measuring the production of NAD^+ over time.

Determination of the TON and TOF values. First the turnover number (TON) and consequently the turnover frequency (TOF) values were calculated by measuring the integrals of a single proton peak belonging both to NAD^+ and NADH (H2 and J2). Then, the percentages of conversion were estimated at different time intervals. TON and TOF were calculated as follow:

$$\mathrm{TON} = \frac{\mathrm{I_{J2}}}{\mathrm{I_{J2}} + \mathrm{I_{H2}}} \; \frac{[\mathrm{NAD^+}]}{[\mathrm{catalyst}]}$$

$$\mathrm{TOF} = \frac{\mathrm{TON}}{\mathrm{hours}}$$

where I_{J2} and I_{H2} are the integral of the NAD^+/NADH protons J2 and H2, and $[NAD^+]$ is the concentration of NAD^+ at the start of the reaction.

DFT calculations. The Gaussian 16 B.01 software[59] was the software of choice. All calculated structures were optimized using the hybrid DFT functional CAM-B3LYP[60] including empirical dispersion with GD3[61] and the basis set CEP-31G[62, 63]. The only exemption was the P atom which has been described with the CEP-31G* basis set including polarization functions. The water solution was simulated via the PCM model[64]. The ΔG energy values of all considered ground and transition states are taken unscaled for 298 K.

Cell lines. MCF-7 (breast adenocarcinoma, ER+), MDA-MB-231 (breast adenocarcinoma, ER-), HT29 (colorectal adenocarcinoma), A549 (lung carcinoma), VERO (cercopithecus aethiops normal kidney) were used in this study. All cell lines were grown at 37 °C in 5% CO_2 atmosphere using DMEM (high glucose) supplemented with 10% foetal calf serum (Gibco® by Life Technologies™), 2 mM L-glutamine (Merck) and 5 µg/mL gentamicin (Gibco® by Life Technologies™).

Antiproliferative assays. Cell viability was assessed using a classical MTT reduction assay. Cells were seeded 24 h before treatment in a sterile 96-well plate (Corning® Costar®, Merck) at cell density of 10000 cells per well (24 h study) or 8000 cells per well (72 h study) to a final volume of 200 µL in DMEM. Cells were treated with a range of compounds at different concentrations (0.03 – 100 µM), all treatments were prepared by serial dilution in DMEM with <0.1% (v/v) DMSO. As a negative control, cells were treated with 0.1% DMSO (v/v). After a further 24 h or 72 h the media was aspirated and replaced with (3-(4,5-dimethylthiazol-2-yl)-2,5-diphenyltetrazolium bromide) (MTT) in PBS (2 mg mL-1) and incubated for 2 h. The solution was then replaced with DMSO to dissolve the formazan crystals and the absorbance at 570 nm was measured on a 96-well plate reader (Infinite® 200 PRO, Tecan). All experiments were performed in triplicate and the average absorbance of DMSO only wells were subtracted from every value. Absorbance values were then plotted against compound concentration. A modified Hill curve fitting function (y = START + (END - START) * x^n / (k^n + x^n)) was then applied using a Levenberg Marquardt fitting algorithm, and an EC_{50} (constant k) was determined for every sample.

Statistical analysis. For less widely used assays the Z-factor (Z-prime) was calculated to confirm the statistical significance of the results. The Z-factor is defined by the means (µ) and standard deviations (δ) of both the positive (p) and negative control (n), in which:

$$\text{Z-factor} = 1 - \frac{3(\delta_p+\delta_n)}{\left|\mu_p-\mu_n\right|}$$

A Z-factor cannot exceed 1 and it was established that any assay which had a Z-factor > 0.5 was suitable for this study. To assess whether a result was statistically significant from the negative control a Student's t-test was used. This test was performed with a two-tailed distribution and two-sample unequal variance. P-values were generated for the null hypothesis that two samples were likely to have come from the same two underlying populations that have the same mean. Statistically significant results were determined to be any p-value ≤ 0.05. Further to this the level of significance was given the following star rating: * = P ≤ 0.05, ** = P ≤ 0.01, *** = P ≤ 0.001.

BODIPY-CHO reduction by fluorescence spectroscopy. BODIPY-CHO and BODIPY-OH were synthesized according to literature procedures[65]. A 3 mL solution containing 30 µM of BODIPY-CHO and 30 µM of NADH was prepared in t-BuOH/H_2O (1:4). This solution was transferred to a quartz cuvette and the initial fluorescence

spectrum was recorded at room temperature. For each sample, 0.2 equiv. of the examined ruthenium catalyst were weighed and added to the cuvette. The fluorescence spectra were recorded every hour for 24 h.

Intracellular transfer hydrogenation catalysis. For live cell imaging, MDA-MB-231 cells were plated in µ-Slide 8-well plates (IBIDI) at a cell density of $5x10^4$ in 300 µL of DMEM per well. After 48 h of cell growth, the medium was removed and wells were replaced with either 30 µM BODIPY-OH solution in DMEM or a 30 µM BODIPY-CHO solution in DMEM. After an incubation time of 4 h (37 °C, 5% CO_2), the BODIPY solutions were removed and all of the cells were rinsed with fresh DMEM (2x300 µL each well). Some BODIPY-CHO treated wells were then incubated with 300 µL of an appropriate ruthenium complex (20 – 30 µM) for 2 h. Afterwards, all medium was removed and cells were rinsed with FluoroBrite™ DMEM (2x300 µL each well). All microscope operations and image processing were conducted using an inverted light microscope (DMi8 Leica, Leica) with a digital camera (Orca Flash 4.0 C11440, Hamamatsu) and a FITC filter cube (Excitation: 460-500 nm, DC: 505, Emission: 592-668 nm, Leica). The gain value for the laser was determined using the BODIPY-OH treated sample and was kept fixed for the acquisition of all images.
Fluorescence image quantification was performed using the program Fiji (ImageJ) by using the formula: corrected total cell fluorescence (CTCF) = [integrated fluorescence density] - [area of selected cell x mean fluorescence of background]. The background fluorescence was calculated by taking the average of five different background regions in a single image. The CTCF was measured for ten cells per well (30 measurements total for each condition). Each set of imaging experiments was performed in triplicate and the final fold-change in fluorescence was relative to the average BODIPY-CHO only control.

Intracellular Reactive Oxygen Species determination. The rate of H_2O_2 production was measured using CM-H2DCFDA (Merck) fluorescent probe. Cells were seeded 48 h before treatment in a sterile 96-well plate (Corning® Costar®, Merck) at cell density of 10000 cells per well to a final volume of 200 µL in DMEM. Afterwards, all medium was removed and replaced with CM-H_2DCFDA (10 µM) in FluoroBrite™ DMEM (200 µL in each well). After an incubation time of 30 min (37 °C, 5% CO_2), the CM-H2DCFDA solutions were removed and the cells were rinsed with FluoroBrite™ DMEM (2x200 µL each well). Some treated wells were then incubated with 300 µL of ruthenium complex or H_2O_2 (50 µM) for 2 h (37 °C, 5% CO_2). Afterwards, the fluorescence emission at 485 nm (bottom surface) was measured on a 96-well plate reader (Infinite® 200 PRO, Tecan). Corrected fluorescence intensity was calculated by subtracting average fluorescence of FluoroBrite™ DMEM only wells. The experiment was repeated 5 times for each complex in each cell line and statistical analysis was performed using the Student's t-test.

NMR spectroscopy of cell metabolite extracts. MCF7 cells were seeded 72 h before extraction in a sterile T75 flask (Thermofisher Scientific). Afterwards, all medium was removed and cells were washed with PBS (2 x 6 mL). Cold MeOH (2 x 3 mL) was then added to the flask and cells were detached using a cell scraper (2 x 1 min). The two methanol solutions were combined and dried under a gentle flow of N_2. Once dry D_2O PBS was added to the off-white solid, vortexed (30 s) and centrifuged (13000 rpm, 4°C, 1 min). The supernatant was incubated with 0.65 ml PBS solution (pD 7.4) of complex **3** (2 mM), transferred into a NMR tube and incubated for 24 h.

Acknowledgements

Authors gratefully acknowledge the DAAD for supporting D.L. with a fellowship. S.R.T. acknowledges TUM Global Postdoctoral Fellowship for funding.

References

1. Robertson, A.; Matsumoto, T.; Ogo, S., The development of aqueous transfer hydrogenation catalysts. *Dalton Transactions* **2011,** *40* (40), 10304-10310.
2. Steckhan, E.; Herrmann, S.; Ruppert, R.; Dietz, E.; Frede, M.; Spika, E., Analytical study of a series of substituted (2,2'-bipyridyl)(pentamethylcyclopentadienyl)rhodium and -iridium complexes with regard to their effectiveness as redox catalysts for the indirect electrochemical and chemical reduction of NAD(P)+. *Organometallics* **1991,** *10* (5), 1568-1577.
3. Lo, H. C.; Leiva, C.; Buriez, O.; Kerr, J. B.; Olmstead, M. M.; Fish, R. H., Bioorganometallic Chemistry. 13. Regioselective Reduction of NAD+ Models, 1-Benzylnicotinamde Triflate and β-Nicotinamide Ribose-5'-methyl Phosphate, with in Situ Generated [Cp*Rh(Bpy)H]+: Structure−Activity Relationships, Kinetics, and Mechanistic Aspects in the Formation of the 1,4-NADH Derivatives. *Inorganic Chemistry* **2001,** *40* (26), 6705-6716.
4. Yan, Y. K.; Melchart, M.; Habtemariam, A.; Peacock, A. F. A.; Sadler, P. J., Catalysis of regioselective reduction of NAD+ by ruthenium(II) arene complexes under biologically relevant conditions. *JBIC Journal of Biological Inorganic Chemistry* **2006,** *11* (4), 483-488.
5. Khan, J. A.; Forouhar, F.; Tao, X.; Tong, L., Nicotinamide adenine dinucleotide metabolism as an attractive target for drug discovery. *Expert Opin Ther Targets* **2007,** *11* (5), 695-705.
6. Ying, W., NAD+/NADH and NADP+/NADPH in cellular functions and cell death: regulation and biological consequences. *Antioxid Redox Signal* **2008,** *10* (2), 179-206.
7. Banerjee, S.; Sadler, P. J., Transfer hydrogenation catalysis in cells. *RSC Chemical Biology* **2021,** *2* (1), 12-29.
8. Chen, F.; Soldevila-Barreda, J. J.; Romero-Canelón, I.; Coverdale, J. P. C.; Song, J.-I.; Clarkson, G. J.; Kasparkova, J.; Habtemariam, A.; Brabec, V.; Wolny, J. A.; Schünemann, V.; Sadler, P. J., Effect of sulfonamidoethylenediamine substituents in RuII arene anticancer catalysts on transfer hydrogenation of coenzyme NAD+ by formate. *Dalton Transactions* **2018,** *47* (21), 7178-7189.
9. Haghdoost, M. M.; Guard, J.; Golbaghi, G.; Castonguay, A., Anticancer Activity and Catalytic Potential of Ruthenium(II)–Arene Complexes with N,O-Donor Ligands. *Inorganic Chemistry* **2018,** *57* (13), 7558-7567.
10. Soldevila-Barreda, J. J.; Bruijnincx, P. C. A.; Habtemariam, A.; Clarkson, G. J.; Deeth, R. J.; Sadler, P. J., Improved Catalytic Activity of Ruthenium–Arene Complexes in the Reduction of NAD+. *Organometallics* **2012,** *31* (16), 5958-5967.
11. Soldevila-Barreda, J. J.; Habtemariam, A.; Romero-Canelón, I.; Sadler, P. J., Half-sandwich rhodium(III) transfer hydrogenation catalysts: Reduction of NAD+ and pyruvate, and antiproliferative activity. *Journal of Inorganic Biochemistry* **2015,** *153*, 322-333.
12. Soldevila-Barreda, J. J.; Romero-Canelón, I.; Habtemariam, A.; Sadler, P. J., Transfer hydrogenation catalysis in cells as a new approach to anticancer drug design. *Nature Communications* **2015,** *6* (1), 6582.
13. Coverdale, J. P. C.; Romero-Canelón, I.; Sanchez-Cano, C.; Clarkson, G. J.; Habtemariam, A.; Wills, M.; Sadler, P. J., Asymmetric transfer hydrogenation by synthetic catalysts in cancer cells. *Nat Chem* **2018,** *10* (3), 347-354.
14. de Torres, M.; Dimroth, J.; Arends, I. W.; Keilitz, J.; Hollmann, F., Towards recyclable NAD(P)H regeneration catalysts. *Molecules* **2012,** *17* (8), 9835-41.
15. Gray, L. R.; Tompkins, S. C.; Taylor, E. B., Regulation of pyruvate metabolism and human disease. *Cellular and Molecular Life Sciences* **2014,** *71* (14), 2577-2604.
16. Coverdale, J. P. C.; Sanchez-Cano, C.; Clarkson, G. J.; Soni, R.; Wills, M.; Sadler, P. J., Easy To Synthesize, Robust Organo-osmium Asymmetric Transfer Hydrogenation Catalysts. *Chemistry – A European Journal* **2015,** *21* (22), 8043-8046.
17. Infante-Tadeo, S.; Rodríguez-Fanjul, V.; Habtemariam, A.; Pizarro, A. M., Osmium(ii) tethered half-sandwich complexes: pH-dependent aqueous speciation and transfer hydrogenation in cells. *Chemical Science* **2021,** *12* (27), 9287-9297.
18. Ganesan, V.; Kim, J. J.; Shin, J.; Park, K.; Yoon, S., Efficient Nicotinamide Adenine Dinucleotide Regeneration with a Rhodium–Carbene Catalyst and Isolation of a Hydride Intermediate. *Inorganic Chemistry* **2022,** *61* (15), 5683-5690.
19. Betanzos-Lara, S.; Liu, Z.; Habtemariam, A.; Pizarro, A. M.; Qamar, B.; Sadler, P. J., Organometallic Ruthenium and Iridium Transfer-Hydrogenation Catalysts Using Coenzyme NADH as a Cofactor. *Angewandte Chemie International Edition* **2012,** *51* (16), 3897-3900.
20. Liu, Z.; Romero-Canelón, I.; Qamar, B.; Hearn, J. M.; Habtemariam, A.; Barry, N. P. E.; Pizarro, A. M.; Clarkson, G. J.; Sadler, P. J., The Potent Oxidant Anticancer Activity of Organoiridium Catalysts. *Angewandte Chemie International Edition* **2014,** *53* (15), 3941-3946.

21. Yang, L.; Bose, S.; Ngo, A. H.; Do, L. H., Innocent But Deadly: Nontoxic Organoiridium Catalysts Promote Selective Cancer Cell Death. *ChemMedChem* **2017,** *12* (4), 292-299.
22. Ngo, A. H.; Ibañez, M.; Do, L. H., Catalytic Hydrogenation of Cytotoxic Aldehydes Using Nicotinamide Adenine Dinucleotide (NADH) in Cell Growth Media. *ACS Catalysis* **2016,** *6* (4), 2637-2641.
23. Jones, W. D.; Kuykendall, V. L.; Selmeczy, A. D., Ring migration reactions of (C5Me5)Rh(PMe3)H2. Evidence for .eta.3 slippage and metal-to-ring hydride migration. *Organometallics* **1991,** *10* (5), 1577-1586.
24. Lo, H. C.; Buriez, O.; Kerr, J. B.; Fish, R. H., Regioselective Reduction of NAD+ Models with [Cp*Rh(bpy)H]+: Structure–Activity Relationships and Mechanistic Aspects in the Formation of the 1,4-NADH Derivatives. *Angewandte Chemie International Edition* **1999,** *38* (10), 1429-1432.
25. Bucci, A.; Dunn, S.; Bellachioma, G.; Menendez Rodriguez, G.; Zuccaccia, C.; Nervi, C.; Macchioni, A., A Single Organoiridium Complex Generating Highly Active Catalysts for both Water Oxidation and NAD+/NADH Transformations. *ACS Catalysis* **2017,** *7* (11), 7788-7796.
26. Fu, Y.; Romero, M. J.; Habtemariam, A.; Snowden, M. E.; Song, L.; Clarkson, G. J.; Qamar, B.; Pizarro, A. M.; Unwin, P. R.; Sadler, P. J., The contrasting chemical reactivity of potent isoelectronic iminopyridine and azopyridine osmium(ii) arene anticancer complexes. *Chemical Science* **2012,** *3* (8), 2485-2494.
27. Ballico, M.; Alessi, D.; Jandl, C.; Lovison, D.; Baratta, W., Terpyridine Diphosphine Ruthenium Complexes as Efficient Photocatalysts for the Transfer Hydrogenation of Carbonyl Compounds. *Chemistry – A European Journal* **2022,** *n/a* (n/a).
28. Figliolia, R.; Cavigli, P.; Comuzzi, C.; Del Zotto, A.; Lovison, D.; Strazzolini, P.; Susmel, S.; Zuccaccia, D.; Ballico, M.; Baratta, W., CNN pincer ruthenium complexes for efficient transfer hydrogenation of biomass-derived carbonyl compounds. *Dalton Transactions* **2020,** *49* (2), 453-465.
29. Giboulot, S.; Baldino, S.; Ballico, M.; Figliolia, R.; Pöthig, A.; Zhang, S.; Zuccaccia, D.; Baratta, W., Flat and Efficient HCNN and CNN Pincer Ruthenium Catalysts for Carbonyl Compound Reduction. *Organometallics* **2019,** *38* (5), 1127-1142.
30. Giboulot, S.; Baldino, S.; Ballico, M.; Nedden, H. G.; Zuccaccia, D.; Baratta, W., Cyclometalated Dicarbonyl Ruthenium Catalysts for Transfer Hydrogenation and Hydrogenation of Carbonyl Compounds. *Organometallics* **2018,** *37* (13), 2136-2146.
31. Giboulot, S.; Comuzzi, C.; Del Zotto, A.; Figliolia, R.; Lippe, G.; Lovison, D.; Strazzolini, P.; Susmel, S.; Zangrando, E.; Zuccaccia, D.; Baldino, S.; Ballico, M.; Baratta, W., Preparation of monocarbonyl ruthenium complexes bearing bidentate nitrogen and phosphine ligands and their catalytic activity in carbonyl compound reduction. *Dalton Transactions* **2019,** *48* (33), 12560-12576.
32. Baldino, S.; Giboulot, S.; Lovison, D.; Nedden, H. G.; Pöthig, A.; Zanotti-Gerosa, A.; Zuccaccia, D.; Ballico, M.; Baratta, W., Preparation of Neutral trans - cis [Ru(O2CR)2P2(NN)], Cationic [Ru(O2CR)P2(NN)](O2CR) and Pincer [Ru(O2CR)(CNN)P2] (P = PPh3, P2 = diphosphine) Carboxylate Complexes and their Application in the Catalytic Carbonyl Compounds Reduction. *Organometallics* **2021,** *40* (8), 1086-1103.
33. Barbosa, M. I. F.; Correa, R. S.; Bastos, T. M.; Pozzi, L. V.; Moreira, D. R. M.; Ellena, J.; Doriguetto, A. C.; Silveira, R. G.; Oliveira, C. R.; Kuznetsov, A. E.; Malta, V. S.; Soares, M. B. P.; Batista, A. A., Structural isomerism of Ru(ii)-carbonyl complexes: synthesis, characterization and their antitrypanosomal activities. *New Journal of Chemistry* **2017,** *41* (11), 4468-4477.
34. Carnizello, A. P.; Alves, J. M.; Pereira, D. E.; Campos, J. C. L.; Barbosa, M. I. F.; Batista, A. A.; Tavares, D. C., Study of the cytotoxic and genotoxic potential of the carbonyl ruthenium(II) compound, ct-[RuCl(CO)(dppb)(bipy)]PF₆ [dppb = 1,4-bis(diphenylphosphino)butane and bipy = 2,2'-bipyridine], by in vitro and in vivo assays. *Journal of applied toxicology : JAT* **2019,** *39* (4), 630-638.
35. Carnizello, A. P.; Barbosa, M. I. F.; Martins, M.; Ferreira, N. H.; Oliveira, P. F.; Magalhães, G. M.; Batista, A. A.; Tavares, D. C., In vitro and in vivo antitumor activity of a novel carbonyl ruthenium compound, the ct-[RuCl(CO)(dppb)(bipy)]PF-6[dppb=1,4-bis(diphenylphosphine)butane and bipy=2,2'-bipyridine]. *Journal of inorganic biochemistry* **2016,** *164*, 42-48.
36. Lovison, D.; Alessi, D.; Allegri, L.; Baldan, F.; Ballico, M.; Damante, G.; Galasso, M.; Guardavaccaro, D.; Ruggieri, S.; Melchior, A.; Veclani, D.; Nardon, C.; Baratta, W., Enantioselective Cytotoxicity of Chiral Diphosphine Ruthenium(II) Complexes Against Cancer Cells. *Chemistry – A European Journal* **2022,** *28* (33), e202200200.
37. Lovison, D.; Allegri, L.; Baldan, F.; Ballico, M.; Damante, G.; Jandl, C.; Baratta, W., Cationic carboxylate and thioacetate ruthenium(ii) complexes: synthesis and cytotoxic activity against anaplastic thyroid cancer cells. *Dalton Transactions* **2020,** *49* (24), 8375-8388.
38. Peacock, A. F. A.; Habtemariam, A.; Fernández, R.; Walland, V.; Fabbiani, F. P. A.; Parsons, S.; Aird, R. E.; Jodrell, D. I.; Sadler, P. J., Tuning the Reactivity of Osmium(II) and Ruthenium(II) Arene Complexes under Physiological Conditions. *Journal of the American Chemical Society* **2006,** *128* (5), 1739-1748.

39. Peacock, A. F. A.; Habtemariam, A.; Moggach, S. A.; Prescimone, A.; Parsons, S.; Sadler, P. J., Chloro Half-Sandwich Osmium(II) Complexes: Influence of Chelated N,N-Ligands on Hydrolysis, Guanine Binding, and Cytotoxicity. *Inorganic Chemistry* **2007,** *46* (10), 4049-4059.
40. Peacock, A. F. A.; Melchart, M.; Deeth, R. J.; Habtemariam, A.; Parsons, S.; Sadler, P. J., Osmium(II) and Ruthenium(II) Arene Maltolato Complexes: Rapid Hydrolysis and Nucleobase Binding. *Chemistry – A European Journal* **2007,** *13* (9), 2601-2613.
41. Peacock, A. F. A.; Parsons, S.; Sadler, P. J., Tuning the Hydrolytic Aqueous Chemistry of Osmium Arene Complexes with N,O-Chelating Ligands to Achieve Cancer Cell Cytotoxicity. *Journal of the American Chemical Society* **2007,** *129* (11), 3348-3357.
42. van Rijt, S. H.; Peacock, A. F. A.; Johnstone, R. D. L.; Parsons, S.; Sadler, P. J., Organometallic Osmium(II) Arene Anticancer Complexes Containing Picolinate Derivatives. *Inorganic Chemistry* **2009,** *48* (4), 1753-1762.
43. Martínez-Peña, F.; Infante-Tadeo, S.; Habtemariam, A.; Pizarro, A. M., Reversible pH-Responsive Behavior of Ruthenium(II) Arene Complexes with Tethered Carboxylate. *Inorganic Chemistry* **2018,** *57* (9), 5657-5668.
44. Kaesz, H. D.; Saillant, R. B., Hydride complexes of the transition metals. *Chemical Reviews* **1972,** *72* (3), 231-281.
45. Huang, J.; Chen, J.; Gao, H.; Chen, L., Kinetic Aspects for the Reduction of CO2 and CS2 with Mixed-Ligand Ruthenium(II) Hydride Complexes Containing Phosphine and Bipyridine. *Inorganic Chemistry* **2014,** *53* (18), 9570-9580.
46. Waldie, K. M.; Ostericher, A. L.; Reineke, M. H.; Sasayama, A. F.; Kubiak, C. P., Hydricity of Transition-Metal Hydrides: Thermodynamic Considerations for CO2 Reduction. *ACS Catalysis* **2018,** *8* (2), 1313-1324.
47. Lever, A. B. P., Electrochemical parametrization of metal complex redox potentials, using the ruthenium(III)/ruthenium(II) couple to generate a ligand electrochemical series. *Inorganic Chemistry* **1990,** *29* (6), 1271-1285.
48. Wiedner, E. S.; Chambers, M. B.; Pitman, C. L.; Bullock, R. M.; Miller, A. J. M.; Appel, A. M., Thermodynamic Hydricity of Transition Metal Hydrides. *Chemical Reviews* **2016,** *116* (15), 8655-8692.
49. Lim, H. S.; Barclay, D. J.; Anson, F. C., Formal potentials and cyclic voltammetry of some ruthenium-ammine complexes. *Inorganic Chemistry* **1972,** *11* (7), 1460-1466.
50. Bose, S.; Ngo, A. H.; Do, L. H., Intracellular Transfer Hydrogenation Mediated by Unprotected Organoiridium Catalysts. *Journal of the American Chemical Society* **2017,** *139* (26), 8792-8795.
51. *APEX suite of crystallographic software, APEX 3*, Version 2016-9.0, Bruker AXS Inc.
; Madison, Wisconsin, USA, 2016.
52. *SAINT*, Version 8.40A and SADABS, Version 2016/2, Bruker AXS Inc.; Madison, Wisconsin, USA, 2016/2019.
53. Sheldrick, G., SHELXT - Integrated space-group and crystal-structure determination. *Acta Crystallographica Section A* **2015,** *71* (1), 3-8.
54. Sheldrick, G., Crystal structure refinement with SHELXL. *Acta Crystallographica Section C* **2015,** *71* (1), 3-8.
55. Hubschle, C. B.; Sheldrick, G. M.; Dittrich, B., ShelXle: a Qt graphical user interface for SHELXL. *Journal of Applied Crystallography* **2011,** *44* (6), 1281-1284.
56. International Tables for Crystallography. **Dordrecht, The Netherlands, 1992,** *Vol. C (Ed.: A. J. Wilson), Kluwer Academic Publishers*, Tables 6.1.1.4 (pp. 500–502), 4.2.6.8 (pp. 219–222), and 4.2.4.2 (pp. 193–199).
57. Spek, A., PLATON SQUEEZE: a tool for the calculation of the disordered solvent contribution to the calculated structure factors. *Acta Crystallographica Section C* **2015,** *71* (1), 9-18.
58. Macrae, C. F.; Sovago, I.; Cottrell, S. J.; Galek, P. T. A.; McCabe, P.; Pidcock, E.; Platings, M.; Shields, G. P.; Stevens, J. S.; Towler, M.; Wood, P. A., Mercury 4.0: from visualization to analysis, design and prediction. *Journal of Applied Crystallography* **2020,** *53* (1), 226-235.
59. Frisch, M. J.; Trucks, G. W.; Schlegel, H. B.; Scuseria, G. E.; Robb, M. A.; Cheeseman, J. R.; Scalmani, G.; Barone, V.; Petersson, G. A.; Nakatsuji, H.; Li, X.; Caricato, M.; Marenich, A. V.; Bloino, J.; Janesko, B. G.; Gomperts, R.; Mennucci, B.; Hratchian, H. P.; Ortiz, J. V.; Izmaylov, A. F.; Sonnenberg, J. L.; Williams; Ding, F.; Lipparini, F.; Egidi, F.; Goings, J.; Peng, B.; Petrone, A.; Henderson, T.; Ranasinghe, D.; Zakrzewski, V. G.; Gao, J.; Rega, N.; Zheng, G.; Liang, W.; Hada, M.; Ehara, M.; Toyota, K.; Fukuda, R.; Hasegawa, J.; Ishida, M.; Nakajima, T.; Honda, Y.; Kitao, O.; Nakai, H.; Vreven, T.; Throssell, K.; Montgomery Jr., J. A.; Peralta, J. E.; Ogliaro, F.; Bearpark, M. J.; Heyd, J. J.; Brothers, E. N.; Kudin, K. N.; Staroverov, V. N.; Keith, T. A.; Kobayashi, R.; Normand, J.; Raghavachari, K.; Rendell, A. P.; Burant, J. C.; Iyengar, S. S.; Tomasi, J.; Cossi, M.; Millam, J. M.; Klene, M.; Adamo, C.; Cammi, R.; Ochterski, J. W.; Martin, R. L.; Morokuma, K.; Farkas, O.; Foresman, J. B.; Fox, D. J. *Gaussian 16 Rev. C.01*, Wallingford, CT, 2016.

60. Yanai, T.; Tew, D. P.; Handy, N. C., A new hybrid exchange–correlation functional using the Coulomb-attenuating method (CAM-B3LYP). *Chemical Physics Letters* **2004,** *393* (1), 51-57.
61. Grimme, S.; Antony, J.; Ehrlich, S.; Krieg, H., A consistent and accurate ab initio parametrization of density functional dispersion correction (DFT-D) for the 94 elements H-Pu. *The Journal of Chemical Physics* **2010,** *132* (15), 154104.
62. Stevens, W. J.; Basch, H.; Krauss, M., Compact effective potentials and efficient shared-exponent basis sets for the first- and second-row atoms. *The Journal of Chemical Physics* **1984,** *81* (12), 6026-6033.
63. Stevens, W. J.; Krauss, M.; Basch, H.; Jasien, P. G., Relativistic compact effective potentials and efficient, shared-exponent basis sets for the third-, fourth-, and fifth-row atoms. *Canadian Journal of Chemistry* **1992,** *70* (2), 612-630.
64. Tomasi, J.; Mennucci, B.; Cammi, R., Quantum Mechanical Continuum Solvation Models. *Chemical Reviews* **2005,** *105* (8), 2999-3094.
65. Yue, Y.; Guo, Y.; Xu, J.; Shao, S., A Bodipy-based derivative for selective fluorescence sensing of homocysteine and cysteine. *New Journal of Chemistry* **2011,** *35* (1), 61-64.